Targeting the De Novo Purine Synthesis Pathway Through Adenylosuccinate Lyase Depletion Impairs Liver Cancer Growth by Perturbing Mitochondrial Function

HHS Public Access

Author manuscript

Dev Cell. Author manuscript; available in PMC 2022 June 21.

Published in final edited form as:

Dev Cell. 2021 June 21; 56(12): 1742–1755.e4. doi:10.1016/j.devcel.2021.05.008.

A transitory signaling center controls timing of primordial germ cell differentiation

Torsten U. Banisch[1,*], **Maija Slaidina**[1], **Selena Gupta**[1], **Megan Ho**[1], **Lilach Gilboa**[2], **Ruth Lehmann**[1,3,4,*]

[1]Department of Cell Biology, Howard Hughes Medical Institute, Skirball Institute of Biomolecular Medicine, NYU School of Medicine, New York City 10016, USA

[2]formerly at Department of Biological Regulation, Weizmann Institute of Science, Rehovot 7610001, Israel

[3]present address: Whitehead Institute for Biomedical Research, Cambridge 02142, USA

[4]lead contact

SUMMARY

Organogenesis requires exquisite spatio-temporal coordination of cell morphogenesis, migration, proliferation and differentiation of multiple cell types. For gonads, this involves complex interactions between somatic and germline tissues. During *Drosophila* ovary morphogenesis primordial germ cells (PGCs) are either sequestered in stem cell niches and maintained in an undifferentiated germline stem cell state, or transition directly towards differentiation. Here, we identify a mechanism that links hormonal triggers of somatic tissue morphogenesis with PGC differentiation. An early ecdysone pulse initiates somatic swarm cell (SwC) migration, positioning them close to PGCs. A second hormone peak activates Torso-like signal in SwCs, which stimulates the Torso RTK signaling pathway in PGCs promoting their differentiation by de-repression of the differentiation gene *bag of marbles.* Thus, systemic temporal cues generate a transitory signaling center that coordinates ovarian morphogenesis with stem cell self-renewal and differentiation programs, highlighting a more general role for such centers in reproductive and developmental biology.

eTOC blurb

*correspondence: Lehmann@wi.mit.edu, torsten.banisch@nyumc.org.

Author Contributions

Conceptualization, R.L., L.G. and T.U.B.; Methodology, R.L., L.G. and T.U.B.; Investigation, T.U.B., S.G. and M.H.; Software and Resources, M.S.; Writing - Original Draft, T.U.B., L.G., R.L.; Writing - Review & Editing, T.U.B., L.G., R.L., M.S.; Visualization, T.U.B.; Supervision, R.L. and L.G.; Funding acquisition, R.L., L.G. and T.U.B.

Further information and requests for resources and reagents should be directed to and will be fulfilled by the Lead Contact, Ruth Lehmann (Lehmann@wi.mit.edu)

Declaration of Interests

The authors declare no competing interests.

During organogenesis, tissue development must be coordinated with stem cell establishment and differentiation to ensure organ function. Banisch et al. identify a transitory signaling center in *Drosophila* ovaries that couples gonad morphogenesis with stem cell niche formation and the initiation of primordial germ cell differentiation timed by hormone pulses.

Graphical Abstract

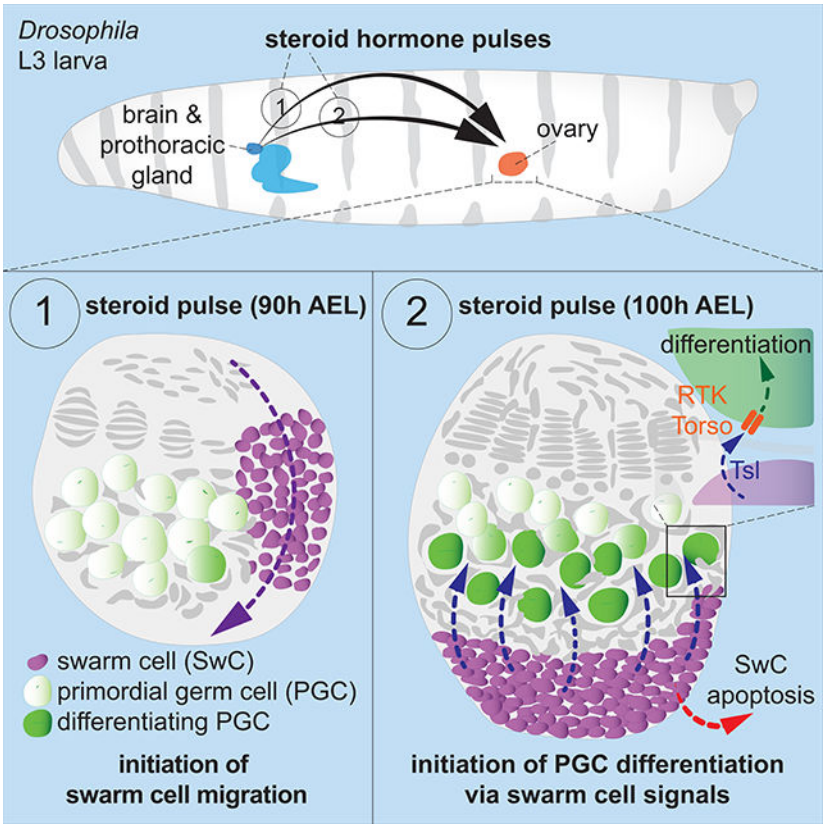

Keywords

gonadogenesis; primordial germ cells; stem cells; morphogenesis; differentiation; germline; swarm cell; ecdysone; steroid hormone; transitory; signaling center; receptor tyrosine kinase; Torso; *Drosophila*

INTRODUCTION

Organ development and function requires complex interactions between cell types, which include the orchestration of proliferation rates, initiation of differentiation and tissue morphogenesis. Such widespread coordination typically requires systemic cues, e.g. hormones, that elicit specific cellular responses and widespread cell-cell signaling events at a given time point (Stamatiades and Kaiser, 2018; Yamanaka et al., 2013). During development, specialized groups of cells can aid in this coordinative effort by inducing cell fate decisions or patterning of surrounding cell types, and thus function as signaling or organizing centers (Anderson and Stern, 2016; Basson, 2012). While hormonal inputs and

downstream signals are known to often act in a transient manner to allow for a stepwise progression of development, it is not well understood how cells perceive and integrate temporal cues and coordinate their response at an organ level.

Such higher-order regulation is exceedingly more complex if developing organs harbor stem cells or their precursors. These must be kept in their naïve, undifferentiated state until their proper niches have formed and they can be maintained as stem cells or their differentiation is initiated. We utilize the developing *Drosophila* ovary as a versatile system to gain insights into the orchestration of cell type specific morphogenesis programs and the coordination of somatic gonad formation with primordial germ cell (PGC) development. A hormonal brain-to-gonad axis has been identified, which coordinates gonadogenesis in *Drosophila*, similar to that in vertebrate systems (Gancz et al., 2011; Hodin and Riddiford, 1998; Sower et al., 2009). Here, distinct peaks of the steroid hormone ecdysone, which is produced in the prothoracic gland (Henrich et al., 1987), dictate the timing of somatic differentiation and maturation and initiate PGC differentiation *via* a yet unknown mechanism. The exploration of this mechanism is the focus of this study.

The *Drosophila* gonads form at the end of embryogenesis when PGCs coalesce with somatic gonadal precursor cells (Boyle and DiNardo, 1995; Sano et al., 2012). During ovarian development, PGCs divide and proliferate in coordination with the directly associated intermingled cells (ICs), while other somatic cell types diversify (Figure 1A) (Gilboa and Lehmann, 2006). An early ecdysone peak between early 3rd larval instar (EL3) and mid 3rd larval instar (ML3) at ~90h AEL (after egg lay) initiates the differentiation of the germline stem cell (GSC) niche: formation of the terminal filaments (TF) and cap cells (CC) (Figure 1A) (Gancz et al., 2011; Warren et al., 2006). The developing somatic niches associate with a fraction of PGCs and subsequently maintain them in an undifferentiated state throughout development and adulthood (Gilboa and Lehmann, 2004; Song et al., 2004; Xie and Spradling, 1998, 2000). GSC maintenance relies on the niche-secreted Bone Morphogenetic Protein (BMP) family ligands Decapentaplegic (Dpp) and Glass bottom boat (Gbb) and on activation of Dpp/Gbb receptors in germ cells. Receptor-mediated phosphorylation of the *Drosophila* SMAD (Mothers against Dpp [Mad]) blocks the germ cell differentiation pathway by binding to the promoter of the key differentiation factor *bag of marbles (bam)* (Chen and McKearin, 2003b; Xie and Spradling, 1998, 2000). However, there are excess PGCs remaining outside the niches that experience only reduced levels of Dpp/Gbb signals. Yet, they do not upregulate *bam* expression and do not initiate differentiation until late 3rd larval instar (LL3). Thus additional, unknown regulators of *bam* transcription that act largely independent of Dpp/Gbb, may mediate the temporal transition toward PGC differentiation. This switch is temporally controlled by a late larval ecdysone pulse (~100h AEL), which is preceding pupal development (Figure 1A) (Gancz et al., 2011; Warren et al., 2006).

It is unclear how PGC differentiation is controlled by ecdysone since PGCs do not express ecdysone receptors. It has therefore been proposed that PGCs interpret ecdysone pulses *via* a secondary cue relayed by somatic cells (Gancz et al., 2011). The identity of the cell type that translates the ecdysone message into a trigger for PGC differentiation and the signaling pathway that transmits and integrates this message remains elusive.

We utilized a recently generated single cell RNA atlas of LL3 ovaries (Slaidina et al., 2020) to search for a relay cell type and the elusive signal. We identified the somatic swarm cells (SwCs) as mediators of the ecdysone signal for posterior gonad formation and PGC differentiation. SwCs constitute a major cell type of the larval gonad that undergoes long distance morphogenetic movements from the anterior to the posterior of the gonad (Couderc et al., 2002). We show that ecdysone has a dual role in SwCs: the early ecdysone pulse initiates SwC morphogenesis and establishes a transitory signaling center. Once SwCs reach the posterior of the gonad, the late pulse induces expression of Torso-like (Tsl) in SwCs, which acts as a soma-to-germline signal to stimulate PGC differentiation. Tsl activates the Torso receptor tyrosine kinase, which in turn releases Krüppel-mediated transcriptional repression of *bam.* Intriguingly, this signaling function of SwCs is limited to a period in development when SwCs are in close proximity to the germline. Thus SwCs act as a transitory signaling center that aids in coupling general gonad morphogenesis with niche establishment and the initiation of PGC differentiation.

RESULTS

SwC migration drives gonad morphogenesis and positions them in close proximity to PGCs.

The *Drosophila* larval gonad at LL3 is comprised of germ cells and of six somatic cell types, the majority of which directly support germline development (Bolivar et al., 2006; Gilboa and Lehmann, 2004, 2006; Slaidina et al., 2020; Xie and Spradling, 2000). The function of SwCs, also called basal cells, during gonadogenesis and their possible contribution to germline development has not been thoroughly analyzed. SwCs originate from the anterior of the gonad, where their numbers are coordinated with terminal filament and sheath cell precursors (Green and Extavour, 2012). During gonad morphogenesis, SwCs move dorso-laterally towards the posterior, where they generate the posterior domain of the ovary (Couderc et al., 2002; King et al., 1968). The timing of their migration and arrival at the posterior coincides with ecdysone peaks. As SwC migration proceeds in close proximity, initially past and then beyond, the location of the PGC population, we reasoned that their orchestrated migration could act as a possible timer for PGC differentiation (Figure 1A, C–E).

To analyze SwC behavior and function, we probed our recently generated single cell RNA sequencing (scRNA-seq.) data-set of LL3 ovaries for SwC signature genes (Slaidina et al., 2020). We identified *single-minded (sim)* and *crossveinless-2 (cv-2)* as highly and quite specifically expressed in SwCs (Figures 1B and S1A, S4A). Antibodies directed against Sim labeled SwC nuclei and allowed us to track them during ovary development. To assess developmental stages accurately and independently of SwC morphogenesis, we used the progression of terminal filament formation labeled with anti-Engrailed (En) antibodies (Figure 1C–E) (Godt and Laski, 1995; Sahut-Barnola et al., 1995). SwCs can be readily detected anterolateral at EL3 (72h AEL) and, at ML3 (96h AEL), on the lateral and dorsal side of the gonad (Figure 1C–D). At LL3 (120h AEL), most SwCs have completed their movements, forming a new posterior domain (Figure 1E) (Couderc et al., 2002). At this position they are in close proximity to posteriorly located PGCs and just below the follicle

stem cell progenitors (FSCPs) as shown by mRNA *in-situ* hybridizations for *sim* and the FSCP marker *bond* (Figure 1F–F') (Slaidina et al., 2020).

To better characterize and genetically manipulate SwCs, we identified Gal4 lines for *sim* and *cv-2* that directed expression in SwCs. Both drivers express in SwCs as early as L2 (Figure 2A) and continue expression throughout their migration (Figure 2B–D). Cv-2-Gal4 showed a broader expression domain than sim-Gal4, including some expression in TFs, CCs and ICs (Figure S1B). Although these driver lines did not label all SwCs (Slaidina et al., 2020), they did recapitulate the expression pattern of endogenous *sim* RNA and therefore provided an excellent tool to analyze SwC behavior and function.

To study the fate of SwCs we used G-TRACE lineage tracing. This method uses a temperature sensitive dual reporter system, where a tissue specific Gal4 drives (1) UAS-FLP recombinase to generate GFP marked clones for lineage labeling by FRT recombination at a defined developmental time and (2) a UAS-fluorescent reporter (RFP) to capture real-time expression patterns (Evans et al., 2009). During larval stages, constitutive expression of the G-TRACE cassette labeled the SwC lineage as early as L2 and throughout their migration (Figure 2A–D). At early pupal stages (36h APF - after puparium formation), SwCs were displaced from the vicinity of germ cells by the expanding layer of FSCPs, labeled by Fasciclin 3 (Fas3) staining (Figure 2E, bracket). At mid-pupal stages (60–72h APF), no current expression of G-TRACE was detected, and SwC descendants were found to contribute to the calyx, a structure connecting the ovary to the oviduct (Figure 2F). Notably, SwC numbers appeared to diminish during pupal stages and cells undergoing programmed cell death were found at the base of developing ovarioles (Figures 2G and S1C). It had been suggested that the contents of these dying cells contribute to the lumen separating individual ovarioles (King et al., 1968). In adults, few SwC descendants were detected in the peritoneal sheath (Figure 2H), when G-TRACE expression was restricted to a brief developmental window from 120h to 144h AEL. This suggests that most SwC descendants are lost during pupal stages. In summary, direct observation and lineage tracing demonstrate that SwCs represent a transitory cell population that comes in close proximity to PGCs. While constituting the most prominent cell population in the larval ovary, they largely disappear during pupal stages with some descendants contributing to the outer ovarian sheath in the adult.

Ecdysone signaling promotes SwC migration.

Our lineage tracing demonstrates that SwCs constitute a transitory cell type that moves from the anterior tip of the ovary to the posterior during larval stages. The formation of this posterior domain has been suggested to depend on ecdysone receptor (EcR) signaling (Gancz et al., 2011). Here, a dominant negative form of EcR, $EcRA^{W650A}$ (from here on EcR^{DN}), which is insensitive to hormone but instead constitutively binds to EcR target genes and represses them, was expressed in all somatic gonadal cells via tj-Gal4. This resulted in a block of PGC differentiation and impaired somatic gonad development and morphogenesis with a range of defects: blocked somatic niche differentiation where the TFs did not form, and CCs were not specified, lack of IC mixing and association with PGCs, and absence of the posterior compartment (Figure S1D–H). When visualized under these conditions, SwC

migration was found to be dramatically affected; SwCs reached a mediolateral position, but failed to migrate towards the posterior (Figure 3A–B).

To investigate whether ecdysone regulates SwC morphogenesis directly, we expressed EcR^{DN} specifically in SwCs via *sim-Gal4* and *cv-2-Gal4.* The resulting SwC morphogenesis defects were similar, albeit less pronounced (Figure 3C–D): the majority of SwCs was found at mediolateral positions in the gonad. SwC numbers were reduced, and we could not detect changes in the number of apoptotic SwCs in EcR^{DN} ovaries (Figure S2A–B), supporting the idea of a continuous requirement of ecdysone for SwC proliferation. Of note, while EcR^{DN} expression greatly affected SwCs, other somatic cell types were unaffected, besides a mild effect on IC intermingling in few ovaries, suggesting the SwC driver lines mainly target and effect SwC function (Figure S1F–H).

To investigate how ecdysone signaling impacts SwC motility we analyzed the morphology of wildtype and EcR^{DN} expressing SwCs at multiple developmental time-points using a microtubule marker (Eb1:GFP). These studies defined three phases of wild type SwC motility: at EL3 (72h), SwCs exhibited clear signs of migratory behavior as judged by their elongated nuclear morphology (Friedl et al., 2011; Kim et al., 2014) and generation of microtubule-rich cellular protrusions towards the direction of movement (Meyen et al., 2015; Ridley, 2011) (Figure 3E). These motility indicators were largely absent at ML3 (96h) when SwCs reached a mediolateral position, but resumed by 98h. At 102h the vast majority of SwCs exhibited morphologies indicative of motility (Figures 3E–G and S2C). Similar to wild type, SwCs expressing EcR^{DN} displayed motile characteristics at EL3 and did not show signs of motility at ML3 when SwCs apparently pause at the mediolateral side of the ovary (Figure 3G). However, in contrast to wild type, EcR^{DN} expressing SwCs did not show any migratory morphologies after ML3 (Figures 3F–G).

Considering the timeline of their migration, this suggests that the early ecdysone cue at ~90h initiates posterior movement of SwCs. A delay of several hours between pulse and tissue response has been noted before (Ashburner, 1990; Regan et al., 2013; Stoiber et al., 2016) and can be explained by the hierarchical expression cascade down-stream of ecdysone, where early response genes activate tissue specific transcriptional programs (Uyehara and McKay, 2019).

SwCs relay Ecdysone signals to initiate timely PGC differentiation.

Discrete pulses of ecdysone initiate diverse developmental processes: the early peak promotes differentiation of the GSC niche and initiates SwC migration, the late peak indirectly initiates PGC differentiation (Figure 1A and S1D–H) (Gancz et al., 2011). Since SwC migration depends on ecdysone and their time of arrival at the gonad posterior aligns well with the initiation of PGC differentiation, we hypothesized that SwCs may relay the late ecdysone peak.

We therefore expressed EcR^{DN} specifically in SwCs and assessed PGC differentiation status at LL3 with a transcriptional reporter for the key differentiation gene *bag of marbles* (bamP:GFP) (Chen and McKearin, 2003b). Under control conditions, *bamP:*GFP expression was detected in PGCs at LL3 (Figure 3H). Signal from the *bamP:*GFP reporter was barely

detectable when EcR^{DN} was expressed in SwCs (Figures 3I–K), suggesting that EcR signaling in SwCs is required for proper timing of PGC differentiation, likely by bringing SwCs into PGC proximity and by inducing expression of a SwC to PGC signal.

In addition to SwCs, ICs presented a possible candidate to transmit the ecdysone signal. ICs are in close proximity to germ cells throughout development, express ecdysone receptors (Figures S1F and S4A) (Gancz et al., 2011; Li et al., 2003) and as escort cells promote germ cell differentiation in the adult (Banisch et al., 2017; Kirilly et al., 2011; Schulz et al., 2002). However, expression of EcR^{DN} in ICs *via* the cell type specific driver *con-G4* (Slaidina et al., 2020) did not result in a block of PGC differentiation (Figure S2D). This result supports our model that SwC are a critical component of the ecdysone-dependent germ cell differentiation signal.

A failure in PGC differentiation in the absence of ecdysone could be caused indirectly because SwCs fail to migrate close to PGCs or, more directly, because SwCs do not produce a differentiation signal. To distinguish between these possibilities, we searched for secondary signaling molecules expressed by SwCs in our scRNA-seq data set (Slaidina et al., 2020), that may specifically affect differentiation but not migration. Based on the PANTHER classification system (Mi et al., 2019) 130 out of 5963 SwC expressed transcripts were predicted to be present on the cell surface or in the extracellular space. Of those, only one transcript, the perforin-like molecule Torso-like (Tsl), was highly enriched in SwCs (Figures 4A and S4A; Methods). RNAi mediated knockdown of *tsl* in SwCs resulted in diminished levels of bamP:GFP, whereas overexpression of *tsl* caused precocious PGC differentiation as evidenced by elevated *bamP:*GFP reporter levels and presence of branched fusomes labeled by anti-α-Spectrin antibodies, a hallmark of germ cell cysts, which are present only at later stages during normal development (Figures 4B–E and S2E) (de Cuevas and Spradling, 1998). These results suggest that Tsl acts as a novel soma to germline signal regulating PGC differentiation status.

To determine whether Tsl functions as a temporal switch for PGC differentiation, we analyzed *tsl* mRNA levels at EL3, ML3 and LL3 using a highly sensitive RNA *in-situ* hybridization chain reaction (HCR) (Choi et al., 2018). While *tsl* mRNA was barely detectable in SwCs at EL3 and ML3, significantly more *tsl* mRNA foci were present at LL3 (Figures 4F–G, S2F–H), suggesting developmental upregulation of *tsl* expression at LL3. *tsl* mRNA was also detected in a few FSCPs at LL3, which is consistent with the scRNA-seq. data (Figure S2H–I). The temporal changes of *tsl* expression were recapitulated with a *tsl* promoter fusion construct (tsl-Gal4) (Grillo et al., 2012). Using the lineage tracing G-TRACE method we found that reporter expression in SwCs was low at ML3 and increased at LL3 (Figures 4H–J). In addition, we compared *tsl* mRNA levels by qPCR from isolated whole ovaries and found that *tsl* expression was increased two-fold from ML3 to LL3. This increase of *tsl* mRNA levels was not detected in EcR^{DN} ovaries, suggesting that initiation of *tsl* expression occurs downstream of ecdysone (Figure 4K). Together, these results suggest that the late ecdysone peak initiates *tsl* expression in SwCs, which promotes PGC differentiation.

To separate ecdysone's early role in SwC migration from a possible later role in relaying a differentiation signal to PGCs, we took advantage of the expression pattern of the tsl-Gal4 driver to block EcR signaling in SwCs. Indeed, late expression of EcR^{DN} (after the early ecdysone peak) *via* tsl-Gal4 left SwC motility intact, allowing them to form a clear posterior domain by LL3 confirming that SwC migration is initiated by the early cue (Figure 4L–M). Importantly, PGCs did not initiate differentiation at LL3 under these conditions, indicating that the late ecdysone signal promotes PGC differentiation via Tsl (Figures 4L–O). In support, tsl-Gal4 driven expression of tsl-RNAi in SwCs blocked PGC differentiation at LL3, while *tsl* overexpression in EcR^{DN} SwCs rescued PGC differentiation defects (Figures 4M–O). Thus, ecdysone-dependent expression of Tsl in SwCs acts as a soma-to-germline signal that is both necessary and sufficient to promote timely PGC differentiation.

Somatic Tsl promotes Torso signaling in PGCs to initiate their timely differentiation.

To determine whether Tsl may be directly acting on PGCs and how it is integrated into the PGC differentiation pathway, we explored the signaling cascade downstream of Tsl. In the fly embryo Tsl facilitates the activation of the receptor tyrosine kinase Torso through its ligand Trunk (Trk) (Casanova et al., 1995; Johnson et al., 2015). While the exact mechanisms by which Tsl exerts its function are still uncertain, the pathway downstream of Torso is well defined and leads via the MAP kinase signaling cascade to the activation of the transcription factors *tailless (tll)* and *huckebein* (*hkb*); these, in turn, instruct the development of the terminal structures of the embryo (Mineo et al., 2018). Consistent with the hypothesis that the complete Torso RTK signaling cascade functions in PGCs (Figure 5A), we detected *torso* and *trk* transcripts specifically in PGCs at LL3 in our scRNA-seq. dataset (Figures S3A–B and S4A) as well as by HCR *in-situ* hybridization (Figure 5B) and qPCR of ML3 and LL3 gonads (Figure S3C). We could also detected the transcript of *tll* in PGCs by HCR (Figure 5B).

To test the involvement of the Torso signaling cascade in this new context, we performed RNAi experiments using the germline specific driver nanos-Gal4. Inhibition of either *torso, trk* or *tll* resulted in decreased *bamP:*GFP levels compared to wild type, suggesting a role in PGC differentiation (Figures 5C–F). Furthermore, expression of an activated version of the ligand Trk $(trk^{[C108]})$ or overexpression of *tll* resulted in precocious differentiation of PGCs outside the somatic niches as early as ML3 (Figures 5G–I and S3D–E). To assess whether Tsl function in PGCs is mediated through the Torso receptor, we made use of a previously described experimentally-induced autocrine mode of Tsl function in embryos (Furriols et al., 1998). Consistent with a role as activator of Torso signaling, overexpression of Tsl in PGCs induced precocious PGC differentiation, while co-expression of Tsl together with torso-RNAi did not (Figure S3F). Together, these results demonstrate that activation of the Torso RTK signaling cascade by SwC-produced Tsl controls the timed differentiation of PGCs that are not incorporated into the somatic niches.

Since Tsl mediated activation of Torso in PGCs parallels its role in the terminal system, we hypothesized that SwC-produced Tsl reaches PGCs in a similar way by diffusion. In support of the idea that Tsl signaling does not require direct cell-cell contact (Henstridge et al., 2018; Sprenger and Nusslein-Volhard, 1992), precocious PGC differentiation occurred already at

ML3 when SwCs are distant from PGCs (Figure S3D–E); furthermore, overexpression of Tsl in EcR^{DN} expressing SwCs, which were located on the mediolateral side of the ovary, did still induce PGC differentiation (Figure S3G–I). Strikingly, the factors shown to be required for Tsl anchoring to the oocyte surface and thereby allowing proper Torso activation *(nasrat, polehole,* and *closca* (Jimenez et al., 2002; Ventura et al., 2010)), were specifically expressed or highly enriched in PGCs based on our scRNA-seq data (Figures S3J–L and S4A). This suggests that PGCs possess a specialized ECM that allows efficient capture of Tsl molecules.

Torso signaling activates key PGC differentiation factor *bam* by relieving Krüppel mediated repression.

Our results show that the temporal control of PGC differentiation is regulated by ecdysone induced expression of Tsl in SwCs, which triggers RTK Torso signaling in PGCs that are not incorporated into stem cell niches. However, it remained unclear how Torso pathway activation is integrated into the PGC differentiation axis ultimately leading to the expression of *bam.* During the ML3 to LL3 transition only a fraction of PGCs is incorporated into newly formed niches and only this fraction is subsequently maintained as GSCs by niche secreted Dpp. PGCs outside the niche experience insufficient levels of Dpp, as indicated by absence of pMad (Zhu and Xie, 2003) and therefore *bam* is not transcriptionally repressed. Yet, these cells do not express *bam* and do not differentiate until induced by the late ecdysone signal (Gancz et al., 2011). This observation raises the possibility that additional, temporally controlled repressors of *bam* transcription act independently of Dpp. We reasoned that activation of the Tsl-Torso cascade at LL3 might relieve this repression. To identify potential repressors, we asked whether targets of the Torso pathway known for their role as repressor during embryogenesis are expressed in larval PGCs. We found that the repressor gene *Krüppel (Kr)* (Gaul and Jackle, 1987; Steingrimsson et al., 1991) is expressed in PGCs at LL3 albeit at very low levels (Figure S4A). Consistent with Kr acting as a repressor of PGC differentiation germline specific *Kr* inhibition by RNAi caused precocious PGC differentiation (Figures 6A–D and S4B–C). Conversely, overexpression of Kr in PGCs effectively blocked *bamP:*GFP reporter expression (Figure 6C–D), suggesting Kr represses the differentiation program in PGCs throughout early larval stages and onwards. Importantly, PGCs in close proximity to the somatic GSC niche were unaffected by expression of Kr-RNAi as judged by normal levels of pMad and absence of *bam*:GFP expression in these cells (Figures 6B and S4D–E). Thus, the somatic niches may secure GSC establishment and maintenance by ‘protecting’ PGCs from the Tsl differentiation signal.

We next investigated whether and how Kr levels are developmentally regulated to allow initiation of PGC differentiation at LL3. HCR *in-situ* hybridizations at EL3, ML3 and LL3 showed that *Kr* mRNA is expressed in PGCs at early stages and is down-regulated by LL3 (Figures 6E and S4F–H), which coincides with the upregulation of *tsl* expression in SwCs. To test whether initiation of Torso signaling cascade represses *Kr* transcription, we compared *Kr* mRNA levels by qPCR in the presence and absence of Tsl. We found that *Kr* mRNA levels remained high at LL3 in *tsl* knock-down conditions, suggesting that *Kr* is regulated by the Tsl-Torso axis (Figure 6F).

Next, we asked whether the effects of Kr on PGC differentiation are mediated by changes in the transcriptional activity of the differentiation gene *bam.* We performed qPCR experiments on whole ovaries at ML3 and LL3. In wild type, *bam* mRNA levels were increased by 10 fold from ML3 to LL3, coinciding with the timing of PGC differentiation (Figure 6G). When overexpressing Kr in PGCs, *bam* transcription was significantly blocked and when expressing RNAi constructs against *Kr,* bam-mRNA levels were already high at ML3 (Figure 6G). These results indicated that Kr inhibits early PGC differentiation by repressing *bam* transcription, possibly by directly controlling the *bam* promoter akin to the Dpp effector Smad (Chen and McKearin, 2003a, 2003b). *In-silico* predictions of transcription factor binding sites in the *bam* promoter revealed a prominent near consensus-binding site for Kr that lies within a promoter region shown to be a critical enhancer element for *bam* transcription (Figure 6H) (Chen and McKearin, 2003b). To test whether this putative Kr binding site functions to regulate *bam* expression we generated transcriptional reporters carrying either the wildtype *bam* promoter sequences ($bamP^{WT}$) or a promoter version with mutations in the predicted Kr binding site ($bamP^{KrMUT}$) (Figure 6H). These reporters were fused to a destabilized version of EGFP, which has a predicted half-life of two hours and thus provides an approximate readout of *bam* transcriptional activity. We detected a significantly higher level of expression from the reporter carrying the mutated Kr binding site than the wildtype construct at LL3, suggesting precocious activation of *bamP* driven transcription (Figures 6I–K). Together our results suggest that Kr is both necessary and sufficient to inhibit PGC differentiation via its role as a repressor of *bam* expression. As for *Kr* RNAi knockdown, *bam* promoter de-repression was only observed in germ cells not associated with the niche, suggesting that the Dpp-Smad pathway can still exert its function on the promoter and acts independently of the Torso-Kr axis.

DISCUSSION

Temporal and spatial coordination of cell proliferation, fate specification and tissue morphogenesis are critical for organogenesis. This interplay between tissues is particularly important during development when stem cells are established within their niches. During this critical period, developing niches may not be fully functional, yet stem cell progenitors have to remain in an undifferentiated state. Our results reveal another aspect of stem cell progenitor control, whereby the differentiation status of cells outside the niche has to be temporally aligned with organogenesis. Our studies identify the somatic SwCs as a critical ecdysone target that transmits a soma to germline differentiation signal. An early ecdysone pulse initiates morphogenetic movements of SwCs from the anterior towards the posterior of the larval gonad. This new position brings SwCs into close contact with PGCs and, in response to a second ecdysone pulse, SwCs then transmit a differentiation signal to PGCs. This signal activates Torso RTK signaling in PGCs, which relieves repression by the transcriptional repressor Krüppel in PGCs, allowing for expression of the germ cell differentiation gene *bam* (Figure 6L).

Hormonal control of gonadogenesis

Steroid-mediated coordination of developmental processes is widely conserved. Pulses of steroid hormones evoke cell type and stage specific outcomes depending on their spatio-

temporal regulation, titer and co-factors. In *Drosophila* gonadogenesis, ecdysone serves a dual role: initiation of early aspects of gonad morphogenesis, such as formation of the somatic niches, SwC morphogenesis to establish a posterior gonadal compartment, and the initiation of PGC differentiation via SwCs ((Gancz et al., 2011); this study).

Akin to ecdysone, in *C. elegans,* the steroid hormone dafrachronic acid (DA) regulates proper gonad morphogenesis, by ensuring correct migration of gonadal leader cells (DTC and LC), which elongate the gonadal arms (Antebi et al., 1998; Motola et al., 2006). DA further promotes germ cell proliferation indirectly at larval stages and has been shown to directly block proliferation of adult germ cells, suggesting a stage specific role of DA in soma and germline development (Mukherjee et al., 2017; Narbonne and Roy, 2006). In mammals, steroidogenic lineages develop only late in development (Herbison, 2016), and the contribution of exogenous signals to early gonadogenesis is less understood. Analogous to ecdysone, Retinoid acid (RA) acts in a concentration dependent manner and binds nuclear receptors that regulate transcriptional programs in germ cells and somatic gonadal cells. In mice, RA is produced in the mesonephros and promotes timely meiotic entry of ovarian germ cells early in development (Bowles et al., 2016, 2006; Chassot et al., 2020; Koubova et al., 2006). Similar to the dual role of ecdysone, RA also regulates somatic gonadal support cell development, the extent of which is under investigation (Bowles et al., 2018; Minkina et al., 2017). In humans, RA directly stimulates germ cell proliferation, differentiation and initiates meiosis of ovarian germ cells (Childs et al., 2011; Le Bouffant et al., 2010). These examples highlight a conserved function of systemic pulsatile cues in gonadogenesis. They act as temporal coordinates and orchestrate somatic gonad formation and germline development. This is in part achieved by promoting expression of secondary cell-cell communicators, which instruct surrounding cells as shown in this study. It remains to be determined how widespread cell-cell signaling in response to steroids/RA is employed in coordinating tissue development, and if similar pathways are involved.

A transient signaling center

Transient signaling centers have been well described in many contexts. Also known as organizing centers, these discrete, specialized groups of cells serve as spatio-temporal point sources for signals that coordinate or evoke developmental processes. These cells, mostly transient in nature, undergo programmed cell death or incorporate into other tissues following their signaling function (Anderson and Stern, 2016; Basson, 2012). We have identified the SwCs as a transitory cell type with signaling capacity in the developing ovary. SwCs play a dual role in ovary development: 1) a structural role, where SwC morphogenesis movements establish the posterior domain of the gonad (Couderc et al., 2002) and likely aid in connecting the ovaries to the oviduct; and 2) a signaling role to promote timely PGC differentiation.

The existence of transitory cell types during gonadogenesis has also been reported in *C. elegans.* The linker cell in *C. elegans* males migrates to elongate the gonad, connects the reproductive tract to the exterior, and undergoes programmed cell death. However, no signaling function has been attributed to the linker cell (Antebi et al., 1997; Hedgecock et al., 1987; Kimble and Hirsh, 1979). In *C. elegans* hermaphrodites, the transitory anchor cell

has pronounced patterning functions. It induces nearby epidermal precursor cells to generate vulval cells, patterns the uterus, and helps establish the physical connection of the epidermis with the uterus (Hill and Sternberg, 1992; Newman et al., 1995, 1996).

In the case of SwCs, it remains to be determined whether they serve as a major signaling hub by relaying signals to other cell types in addition to PGCs. Observations of SwC migration and TF maturation suggest that both processes are coordinated (Figure 1C–E): TF stack formation occurs in a medial to lateral fashion with the least mature TF stack in the vicinity of SwCs (Godt and Laski, 1995; Sahut-Barnola et al., 1996), and a block in SwC migration and concomitant increase in SwC numbers has been shown to negatively impact the number of TFs formed (Green and Extavour, 2012). This coordination may involve SwC signals.

Regulatory hierarchies for stem cell maintenance and differentiation

We identified a new signaling module in PGCs that regulates the timing of PGC differentiation. Our findings suggest that Kr functions in parallel to the well-established Dpp/pMad mediated signaling pathway throughout larval development (Gilboa and Lehmann, 2004; Song et al., 2004; Xie and Spradling, 1998, 2000). Both pathways block precocious PGC differentiation, however their actions are regulated in time and space. Before ML3, both Dpp-mediated signaling and Kr repress differentiation throughout the PGC compartment; from ML3 (96h AEL) the reach of Dpp becomes progressively restricted to the proximity of the newly formed niches to maintain a fraction of PGCs as GSCs for adulthood (Gancz and Gilboa, 2013; Gilboa and Lehmann, 2004; Song et al., 2002; Zhu and Xie, 2003). Precocious differentiation of PGCs outside the niches, which are not exposed to Dpp, is continuously repressed by Kr until mid-LL3 (~108h AEL) when the Torso pathway is activated and *bam* expression is first detected in PGCs (Gancz et al., 2011).

This dual repression system keeps PGCs in an uncommitted state to accommodate the complexity of somatic gonad morphogenesis. This allows formation of a functional niche, generation of a posterior compartment, and FSCP specification and positioning before initiating the first round of germline cyst formation (Gilboa, 2015; Slaidina et al., 2020). Any failures in this temporal and physical coordination are detrimental to fecundity as precocious PGC differentiation decreases the pool of future GSCs (Gancz et al., 2011; Wang and Lin, 2004). Moreover, a significant increase in *bamP:GFP* positive germ cell cysts that were not incorporated into the germarium was detected at pupal stages in ovaries where PGCs differentiated precociously, suggesting these germ cells do not contribute to egg chamber formation and will likely undergo apoptosis (Figure S4I–J).

This dual repression system is integrated at the level of the *bam* promoter. A Kr binding site responsive to Torso signaling, is located within a critical enhancer element of the *bam* promoter. Removal of this element results in low *bam* expression, suggesting Kr gates *bam* expression and does not fully abrogate expression as exerted by pMad/Medea (Chen and McKearin, 2003a, 2003b). In line with the suggested mode of Kr function as a local quenching factor for nearby activators (Gray and Levine, 1996), we hypothesize that Kr interaction with this enhancer element blocks access to the *bam* promoter for still elusive transcriptional activators.

Limitations of the Study

Our study suggest that Tsl mediates PGC differentiation by facilitating the activation of the Torso receptor kinase. It is unclear how the Tsl signal is efficiently transmitted to PGCs. We do not think that direct contact with PGCs is required, although we have observed this in some cases. It is likely that PGCs employ a specialized ECM as indicated in the manuscript, but we have not directly tested this possibility. If direct SwC contact with PGCs is not required for activation, it is curious why GSCs in the somatic niche remain in an undifferentiated state and appear unresponsive from receiving the Tsl signal. One possibility is that the reach of Tsl is limited to PGCs and may even be actively excluded from GSCs. Alternatively, as discussed above, high levels of Dpp in the niche may dominate and maintain transcriptional silencing of the *bam* promoter.

In this study we used a con-Gal4 driver line to specifically target ICs. We identified con as a gene specifically expressed in IC cells by single cell RNA-seq (Slaidina et al., 2020). Con-Gal4 is the only driver we identified showing IC specific expression (Tirian and Dickson, 2017). In our analysis we found that con-Gal4 drives expression only in a few ICs (Slaidina et al., 2020). Thus, its usefulness might be limited and a thorough examination of the contribution of ICs to germline development will require more robustly expressed IC driver lines.

STAR Methods

RESOURCE AVAILABILITY Lead Contact

Information regarding requests for materials used in this paper are listed in the Key Resources Table. Further information and requests for reagents, protocols or other resources should be directed and will be fulfilled by the lead contact, Ruth Lehmann (Lehmann@wi.mit.edu).

Materials Availability—Plasmids, fly stocks generated for this study are listed in the Key Resources Table and available from the lead contact.

Data and Code availability—The single cell RNA sequencing data set used in this study has been published and all associated data are available in (Slaidina et al., 2020) and in GEO under accession code GSE131971.

EXPERIMENTAL MODEL AND SUBJECT DETAILS

Drosophila melanogaster were raised on medium containing yeast, molasses and cornmeal, and kept at 25°C. A complete list of fly lines used in this study can be found in the Key Resources Table.

Staging: To obtain flies of similar developmental stages, care was taken to work with under-crowded cultures. Flies were transferred into a fresh vial to lay eggs for 3h, and were then removed. Vials were left at 25° for 48h (second larval instar), 72h (early third larval instar) for 96 h (mid third instar, ML3) or 120 h (late third instar, LL3). Under these conditions the development of wildtype gonads is uniform. Strictly following this laying

regiment, the differences in staging are kept at a minimum: EL3 labeled gonads used in this study range from 69–72h AEL, ML3 labeled gonads range from 93–96h AEL and LL3 labeled gonads range from 117–120h AEL.

To further account for staging differences, all gonads were co-stained with DAPI and TF maturation status, overall ovary size, as determined by eye on the individual slide was used as proxy to verify accurate staging. After establishment of the SwC migration timeline, their position within the ovary was also considered for staging. The terminology we use is according to Ashburner (Ashburner, 1989).

METHODS DETAIL

Dissections—Larvae were dissected as described previously (Maimon and Gilboa, 2011). In short: Larvae were rinsed in Ringer's solution or DPBS (for *in situ* hybridization). Heads were removed with forceps. Specimens were inverted and trachea and guts were gently removed. For *in situ* and EL3 stages the fatbody was left attached to the cuticle, for all other purposes the cuticle was removed prior to staining. Properly staged pupae were dissected following the procedures in (Park et al., 2018). For adults, females were dissected 3 days after eclosion with 1 day fattening on yeast. Abdomens were removed using forceps, intestine was removed and staining was done with the ovaries partly covered by the abdominal cuticle.

Immunofluorescence staining—All steps were performed with gentle rotation. Specimens were fixed in Ringer's solution, 4% Paraformaldehyde for 20min at RT, followed by a short wash with 1% PBT (TritonX in PBS), and 1h wash in PBT for permeabilization. Blocking was done in 0.3% PBTB (TritonX in 1% BSA) for at least 1h at RT. Primary antibodies were incubated at 4°C, overnight in 0.3% PBTB. Subsequently, specimens were washed twice for 30min with 0.3% PBTB, followed by 1h in 0.3% PBTB. Secondary antibodies were diluted in 0.3% PBTB and incubated for 2h at RT, followed by three washes in 0.3%PBT (TritonX in PBS). For mounting, specimens were equilibrated in Vectashield+ DAPI and the fatbody was removed from the gonads with dissecting needles.

RNA *in situ* hybridization—All steps are done in using RNAse free reagents and supplies and with gentle rotation, except for steps at 37°C. The protocol was adapted from (Choi et al., 2018). Specimens were fixed in PBS, Tween (Tw) 0.1%, Paraformaldehyde 4% for 20 minutes at RT, washed twice with PBS, Tw 0.1% at RT, dehydrated with sequential washes with 25%, 50%, 75% and 100% methanol in PBS on ice 5 minutes each. Samples were stored at −20°C at least overnight (up to one week). Samples were rehydrated with sequential washes with 100%, 75%, 50% and 25% methanol in PBS on ice, permeated for 2 hours in PBS Tx 1% at RT, post-fixed in PBS, Tw 0.1%, Paraformaldehyde 4% for 20 minutes at RT, washed twice with PBS, Tw 0.1% for 5 minutes on ice, washed with 50% PBS, Tw 0.1%/ 50% 5xSSCT (5xSSC, Tween 0.1%) for 5 minutes on ice, washed twice with 5xSSCT for 5 minutes on ice, incubate in probe hybridization buffer for 5 minutes on ice, pre-hybridized in probe hybridization buffer for 30 minutes at 37° C, and hybridized overnight at 37°C. Probe concentrations were determined empirically, and ranged 4 – 8 pmol of each probe in 1 ml. Probe solution was prepared by adding probes to pre-warmed probe

hybridization solution. After hybridization, specimens were washed 4 times with probe wash buffer for 15 minutes each at 37°C, and twice with 5xSSCT for 5 minutes each at RT. Specimens were equilibrated in amplification buffer for 5 minutes at RT. Hairpin solutions were prepared by heating 30 pmol of each hairpin for 90 seconds at 95°C and cooling at RT in a the dark for 30 minutes, and subsequently adding the snap-cooled hairpins to 500 µl of amplification buffer at RT. Specimens were incubated in hairpin solution overnight at RT, and washed multiple times with 5xSSCT - twice for 5 minutes, twice for 30 minutes and once for 5 minutes. DAPI was added in the first 30-minute wash. Specimens were either equilibrated in Vectashield overnight at 4°C and mounted in Vectashield, or subsequent immunofluorescence staining was carried out (see above).

Detection of mRNA foci—After the HCR *in-situ* protocol (see above), gonads were scanned on the confocal microscope, a volume of 5 µm in 1 µm z-plane step was acquired. Stacks were maximum projected in Fiji software. Area of SwCs *(sim* signal) or PGCs (vasa signal) was outlined and area around this ROI removed (Fiji edit>clear outside). Nuclei contained in the area were counted manually (DAPI signal) to determine SwC/PGC numbers. mRNA abundance was determined using the freely available spot-detection algorithm (Airlocalize) as described in (Trcek et al., 2017), which was developed in the MATLAB programming language (MathWorks) by (Lionnet et al., 2011). Briefly: batch mode analysis of 2d images was performed. To increase spot detection accuracy initial settings for the analysis were determined on a smaller ROI in an image file; a generated image of such detected spots was overlaid with the original image file to confirm accuracy. An intensity histogram of identified mRNA spots was plotted, and a mean intensity value determined by Gaussian distribution and by verification of high and low values to actual mRNA spots in the image file. Spots around the mean intensity (1): > 0.5 = 1 < 1.5 were counted as single mRNA foci; < 0.5 as background and > 1.5 stepwise as 2, 3 foci etc. Notably, mRNA spots detected *via* the software likely present single RNA molecules, however since HCR amplifies the signal from used probes we refer to these spots as mRNA foci. Since we assume that HCR amplification is even across detected mRNAs we assign higher than mean pixel intensity values to more than one mRNA foci. The number of mRNA foci obtained for a single ovary was divided by the number of cells (SwCs or PGCs) counted for this particular ovary to obtain the plotted mean per cell value.

Imaging and image analysis—Images were acquired using Zeiss LSM 800 and 780 confocal microscopes using 40x oil NA 1.3 objectives. Confocal images shown are maximum projections of 3z-planes 1µm apart.

scRNA-seq data—For detailed description of the LL3 ovary scRNA-seq. data please refer to (Slaidina et al., 2020). The scRNA-seq data set is available in GEO under accession code GSE131971. For prediction of SwC expressed genes, a lower cut off of 0.05 (average gene expression per cell type) was chosen.

The underlying gene expression values were generated by log-normalization using a scale factor of 10000 molecules for each cell, and further standardization for each gene across all cells (z-score transformed) (Butler et al., 2018). The cut off was determined by comparing expression values of germline specific markers (e.g. *vasa, brul, ovo)* in somatic tissues to

define noisy expression levels. *tsl* was identified from a list of genes that are (a) SwC expressed and (b) predicted to be signaling molecules or extracellular components; and (c) *tsl* was 7.5-fold enriched in SwCs compared to other cell types, while the next candidates on that list were *CG30287* and *egr,* which showed 2.4-fold and no enrichment respectively.

Lineage tracing—Lineage specific expression of *sim*-Gal4 and *cv-2*-Gal4 was validated by expression of a G-TRACE cassette. Positively marked cells were followed from L2 to late pupal stages. To lineage trace SwCs marked at LL3 into adult stages, temperature shifts utilizing the Gal80ts system were performed. Larvae were raised in the restrictive temperature (25°) till 120h-144h AEL and subsequently shifted to the permissive temperature (18°). Adults were dissected 1d after eclosion.

SwC motility index—Gonads were dissected and IHC performed at 72h, 96h, 98h, 100h and 102h. Subsequently, SwCs positively marked by *sim-G4>Ebl:GFP* were analyzed. For each SwC, 'motile morphology' was determined, where a motile cell is defined as having both, cellular protrusions generated towards the gonad posterior and elongated nuclear morphology. Both parameters were scored visually, with DAPI marking nuclei and Eb1:GFP labeling protrusions. 8% of analyzed SwCs displayed only one migratory parameter and were scored as non-motile. These might be stationary cells with protrusions generated in random directions or migratory cells in the process of reorienting their motile machinery.

qPCR analysis—Larva dissections were carried out as described previously (Gancz and Gilboa, 2017). Extracted, whole ovaries (germline and somatic tissues) were frozen in liquid nitrogen and stored at −80°C for one day. For best RNA yield, 15–20 gonads of LL3 and 25 gonads of ML3 were used. RNA extraction was done using RNeasy micro Kit from Qiagen following manufacturers protocol; followed by cDNA synthesis with Supercript IV from Invitrogen. mRNA levels of *rps17* served as a control. To further test whether temporal control via ecdysone was limited to *tsl* mRNA expression, qPCRs for *trunk*- and *torso* mRNA levels were performed and showed no change from ML3 to LL3 (Figure S3C). qPCR analysis was performed on a Roche LightCycler 480 II system.

Differentiation assay - *bamP:GFP* levels—Ovaries for wildtype and experiment were dissected, stained and imaged at the same time with the same settings throughout. For confocal imaging, a volume encompassing all germ cells was acquired. Subsequent analysis was performed in Fiji. The ten brightest germ cells per gonad were determined visually; ROI outlined in Fiji and mean pixel intensity values measured. The plotted relative intensity values represent the ratio of measured values and the mean wildtype value of the same experiment. For each experiment up to 10 gonads were imaged and each experimental condition was repeated at least three times.

QUANTIFICATION AND STATISTICAL ANALYSIS

All experiments were performed with at least three biological repeats. For all experiments, over 25 ovaries were examined. Statistical significance was determined using Mann-Whitney L-test. Error bars represent standard deviation (SD). n values given indicate number of ovaries or number of cells examined, and are specifically explained in the figure legends.

Supplementary Material

Refer to Web version on PubMed Central for supplementary material.

Acknowledgements

We would like to thank Drs. Jordi Casanova, Michael Buszczak, Dorothea Godt, Erika Bach, Jessica Treisman, Stephen Crews and Katsuo Furukubo-Tokunaga for kindly sharing their reagents. We thank the TRiP at Harvard Medical School for providing transgenic RNAi fly stocks used in this study. We thank the Bloomington Drosophila Stock Center (NIH P40OD018537), the Vienna Drosophila resource center (VDRC), the Kyoto Stock Center (DGRC) and FlyORF stock collections for the stocks used in this study. We acknowledge the FlyBase team for their exceptional work on the *Drosophila* database. We thank Shifra Ben-Dor at the Life Sciences Core Facilities at the Weizmann Institute of Science for *in-silico* prediction of Krüppel binding sites in the *bam* promoter. We thank Drs. Dana Meyen and Toby Lieber for critical review of the manuscript and all members of the Lehmann lab for helpful discussions, constructive comments and ideas.

Funding

T.U.B. was supported by a European Molecular Biology Organisation long-term fellowship (ALTF47-2014). M.S. was a Howard Hughes Medical Institute (HHMI) Fellow of the Life Sciences Research Foundation. S.G. and M.H. are supported by NYU Dean's Undergraduate Research Fund Grants. L.G. was supported by Israel Cancer Research Fund (12-3073-PG) and by the Helen and Martin Kimmel Institute for Stem Cell Research at the Weizmann Institute of Science (HMKISCR). Research in the Lehmann lab was supported by HHMI, where R.L. was an investigator, and by NIH R37HD41900.

References

Anderson C, and Stern CD (2016). Organizers in Development. Curr Top Dev Biol 117, 435–454. [PubMed: 26969994]

Antebi A, Culotti JG, and Hedgecock EM (1998). daf-12 regulates developmental age and the dauer alternative in Caenorhabditis elegans. Development 125, 1191–1205. [PubMed: 9477318]

Antebi A, Norris CR, Hedgecock EM, and Garriga G (1997). Cell and Growth Cone Migrations. In elegans C II, nd, Riddle DL, Blumenthal T, Meyer BJ, and Priess JR, eds. (Cold Spring Harbor (NY)).

Ashburner M (1989). Drosophila. A laboratory handbook (Cold spring harbor laboratory press). Ashburner, M. (1990). Puffs, genes, and hormones revisited. Cell 61, 1–3.

Banisch TU, Maimon I, Dadosh T, and Gilboa L (2017). Escort cells generate a dynamic compartment for germline stem cell differentiation via combined Stat and Erk signalling. Development 144, 1937–1947. [PubMed: 28559239]

Basson MA (2012). Signaling in cell differentiation and morphogenesis. Cold Spring Harbor perspectives in biology 4.

Bischof J, Bjorklund M, Furger E, Schertel C, Taipale J, and Basler K (2013). A versatile platform for creating a comprehensive UAS-ORFeome library in Drosophila. Development 140, 2434–2442. [PubMed: 23637332]

Bolivar J, Pearson J, Lopez-Onieva L, and Gonzalez-Reyes A (2006). Genetic dissection of a stem cell niche: the case of the Drosophila ovary. Dev Dyn 235, 2969–2979. [PubMed: 17013875]

Bowles J, Feng CW, Ineson J, Miles K, Spiller CM, Harley VR, Sinclair AH, and Koopman P (2018). Retinoic Acid Antagonizes Testis Development in Mice. Cell Rep 24, 1330–1341. [PubMed: 30067986]

Bowles J, Feng CW, Miles K, Ineson J, Spiller C, and Koopman P (2016). ALDH1A1 provides a source of meiosis-inducing retinoic acid in mouse fetal ovaries. Nat Commun 7, 10845. [PubMed: 26892828]

Bowles J, Knight D, Smith C, Wilhelm D, Richman J, Mamiya S, Yashiro K, Chawengsaksophak K, Wilson MJ, Rossant J, et al. (2006). Retinoid signaling determines germ cell fate in mice. Science 312, 596–600. [PubMed: 16574820]

Boyle M, and DiNardo S (1995). Specification, migration and assembly of the somatic cells of the Drosophila gonad. Development 121, 1815–1825. [PubMed: 7600996]

Brand AH, and Perrimon N (1993). Targeted gene expression as a means of altering cell fates and generating dominant phenotypes. Development 118, 401–415. [PubMed: 8223268]

Butler A, Hoffman P, Smibert P, Papalexi E, and Satija R (2018). Integrating single-cell transcriptomic data across different conditions, technologies, and species. Nat Biotechnol 36, 411–420. [PubMed: 29608179]

Casali A, and Casanova J (2001). The spatial control of Torso RTK activation: a C-terminal fragment of the Trunk protein acts as a signal for Torso receptor in the Drosophila embryo. Development 128, 1709–1715. [PubMed: 11290307]

Casanova J, Furriols M, McCormick CA, and Struhl G (1995). Similarities between trunk and spatzle, putative extracellular ligands specifying body pattern in Drosophila. Genes & development 9, 2539–2544. [PubMed: 7590233]

Chassot AA, Le Rolle M, Jolivet G, Stevant I, Guigonis JM, Da Silva F, Nef S, Pailhoux E, Schedl A, Ghyselinck NB, et al. (2020). Retinoic acid synthesis by ALDH1A proteins is dispensable for meiosis initiation in the mouse fetal ovary. Sci Adv 6, eaaz1261. [PubMed: 32494737]

Chen D, and McKearin D (2003a). Dpp signaling silences bam transcription directly to establish asymmetric divisions of germline stem cells. Current biology : CB 13, 1786–1791. [PubMed: 14561403]

Chen D, and McKearin DM (2003b). A discrete transcriptional silencer in the bam gene determines asymmetric division of the Drosophila germline stem cell. Development 130, 1159–1170. [PubMed: 12571107]

Childs AJ, Cowan G, Kinnell HL, Anderson RA, and Saunders PT (2011). Retinoic Acid signalling and the control of meiotic entry in the human fetal gonad. PloS one 6, e20249. [PubMed: 21674038]

Choi HMT, Schwarzkopf M, Fornace ME, Acharya A, Artavanis G, Stegmaier J, Cunha A, and Pierce NA (2018). Third-generation in situ hybridization chain reaction: multiplexed, quantitative, sensitive, versatile, robust. Development 145.

Couderc JL, Godt D, Zollman S, Chen J, Li M, Tiong S, Cramton SE, Sahut-Barnola I, and Laski FA (2002). The bric a brac locus consists of two paralogous genes encoding BTB/POZ domain proteins and acts as a homeotic and morphogenetic regulator of imaginal development in Drosophila. Development 129, 2419–2433. [PubMed: 11973274]

de Cuevas M, and Spradling AC (1998). Morphogenesis of the Drosophila fusome and its implications for oocyte specification. Development 125, 2781–2789. [PubMed: 9655801]

Evans CJ, Olson JM, Ngo KT, Kim E, Lee NE, Kuoy E, Patananan AN, Sitz D, Tran P, Do MT et al. (2009). G-TRACE: rapid Gal4-based cell lineage analysis in Drosophila. Nat Methods 6, 603–605. [PubMed: 19633663]

Friedl P, Wolf K, and Lammerding J (2011). Nuclear mechanics during cell migration. Curr Opin Cell Biol 23, 55–64. [PubMed: 21109415]

Furriols M, Casali A, and Casanova J (1998). Dissecting the mechanism of torso receptor activation. Mech Dev 70, 111–118. [PubMed: 9510028]

Furriols M, Ventura G, and Casanova J (2007). Two distinct but convergent groups of cells trigger Torso receptor tyrosine kinase activation by independently expressing torso-like. Proceedings of the National Academy of Sciences of the United States of America 104, 11660–11665. [PubMed: 17595301]

Gancz D, and Gilboa L (2013). Insulin and Target of rapamycin signaling orchestrate the development of ovarian niche-stem cell units in Drosophila. Development 140, 4145–4154. [PubMed: 24026119]

Gancz D, and Gilboa L (2017). RNA Isolation from Early Drosophila Larval Ovaries. Methods Mol Biol 1463, 75–83. [PubMed: 27734348]

Gancz D, Lengil T, and Gilboa L (2011). Coordinated regulation of niche and stem cell precursors by hormonal signaling. PLoS biology 9, e1001202. [PubMed: 22131903]

Gaul U, and Jackle H (1987). Pole region-dependent repression of the Drosophila gap gene Kruppel by maternal gene products. Cell 51, 549–555. [PubMed: 3119224]

Gilboa L (2015). Organizing stem cell units in the Drosophila ovary. Current opinion in genetics & development 32, 31–36. [PubMed: 25703842]

Gilboa L, and Lehmann R (2004). Repression of primordial germ cell differentiation parallels germ line stem cell maintenance. Current biology : CB 14, 981–986. [PubMed: 15182671]

Gilboa L, and Lehmann R (2006). Soma-germline interactions coordinate homeostasis and growth in the Drosophila gonad. Nature 443, 97–100. [PubMed: 16936717]

Godt D, and Laski FA (1995). Mechanisms of cell rearrangement and cell recruitment in Drosophila ovary morphogenesis and the requirement of bric a brac. Development 121, 173–187. [PubMed: 7867498]

Gray S, and Levine M (1996). Short-range transcriptional repressors mediate both quenching and direct repression within complex loci in Drosophila. Genes & development 10, 700–710. [PubMed: 8598297]

Green DA 2nd, and Extavour CG (2012). Convergent evolution of a reproductive trait through distinct developmental mechanisms in Drosophila. Developmental biology 372, 120–130. [PubMed: 23022298]

Grillo M, Furriols M, de Miguel C, Franch-Marro X, and Casanova J (2012). Conserved and divergent elements in Torso RTK activation in Drosophila development. Scientific reports 2, 762. [PubMed: 23094137]

Hedgecock EM, Culotti JG, Hall DH, and Stern BD (1987). Genetics of cell and axon migrations in Caenorhabditis elegans. Development 100, 365–382. [PubMed: 3308403]

Henrich VC, Tucker RL, Maroni G, and Gilbert LI (1987). The ecdysoneless (ecd1ts) mutation disrupts ecdysteroid synthesis autonomously in the ring gland of Drosophila melanogaster. Developmental biology 120, 50–55. [PubMed: 3102296]

Henstridge MA, Aulsebrook L, Koyama T, Johnson TK, Whisstock JC, Tiganis T, Mirth CK, and Warr CG (2018). Torso-Like Is a Component of the Hemolymph and Regulates the Insulin Signaling Pathway in Drosophila. Genetics 208, 1523–1533. [PubMed: 29440191]

Herbison AE (2016). Control of puberty onset and fertility by gonadotropin-releasing hormone neurons. Nat Rev Endocrinol 12, 452–466. [PubMed: 27199290]

Hill RJ, and Sternberg PW (1992). The gene lin-3 encodes an inductive signal for vulval development in C. elegans. Nature 358, 470–476. [PubMed: 1641037]

Hodin J, and Riddiford LM (1998). The ecdysone receptor and ultraspiracle regulate the timing and progression of ovarian morphogenesis during Drosophila metamorphosis. Dev Genes Evol 208, 304–317. [PubMed: 9716721]

Jimenez G, Gonzalez-Reyes A, and Casanova J (2002). Cell surface proteins Nasrat and Polehole stabilize the Torso-like extracellular determinant in Drosophila oogenesis. Genes & development 16, 913–918. [PubMed: 11959840]

Johnson TK, Henstridge MA, Herr A, Moore KA, Whisstock JC, and Warr CG (2015). Torso-like mediates extracellular accumulation of Furin-cleaved Trunk to pattern the Drosophila embryo termini. Nat Commun 6, 8759. [PubMed: 26508274]

Kim DH, Cho S, and Wirtz D (2014). Tight coupling between nucleus and cell migration through the perinuclear actin cap. J Cell Sci 127, 2528–2541. [PubMed: 24639463]

Kimble J, and Hirsh D (1979). The postembryonic cell lineages of the hermaphrodite and male gonads in Caenorhabditis elegans. Developmental biology 70, 396–417. [PubMed: 478167]

King RC, Aggarwal SK, and Aggarwal U (1968). The development of the female Drosophila reproductive system. J Morphol 124, 143–166. [PubMed: 5654408]

Kirilly D, Wang S, and Xie T (2011). Self-maintained escort cells form a germline stem cell differentiation niche. Development 138, 5087–5097. [PubMed: 22031542]

Koubova J, Menke DB, Zhou Q, Capel B, Griswold MD, and Page DC (2006). Retinoic acid regulates sex-specific timing of meiotic initiation in mice. Proceedings of the National Academy of Sciences of the United States of America 103, 2474–2479. [PubMed: 16461896]

Le Bouffant R, Guerquin MJ, Duquenne C, Frydman N, Coffigny H, Rouiller-Fabre V, Frydman R, Habert R, and Livera G (2010). Meiosis initiation in the human ovary requires intrinsic retinoic acid synthesis. Hum Reprod 25, 2579–2590. [PubMed: 20670969]

Lee PT, Zirin J, Kanca O, Lin WW, Schulze KL, Li-Kroeger D, Tao R, Devereaux C, Hu Y, Chung V, et al. (2018). A gene-specific T2A-GAL4 library for Drosophila. eLife 7.

Li MA, Alls JD, Avancini RM, Koo K, and Godt D (2003). The large Maf factor Traffic Jam controls gonad morphogenesis in Drosophila. Nature cell biology 5, 994–1000. [PubMed: 14578908]

Lionnet T, Czaplinski K, Darzacq X, Shav-Tal Y, Wells AL, Chao JA, Park HY, de Turris V, Lopez-Jones M, and Singer RH (2011). A transgenic mouse for in vivo detection of endogenous labeled mRNA. Nat Methods 8, 165–170. [PubMed: 21240280]

Maimon I, and Gilboa L (2011). Dissection and staining of Drosophila larval ovaries. J Vis Exp.

McGuire SE, Le PT, Osborn AJ, Matsumoto K, and Davis RL (2003). Spatiotemporal rescue of memory dysfunction in Drosophila. Science 302, 1765–1768. [PubMed: 14657498]

Meyen D, Tarbashevich K, Banisch TU, Wittwer C, Reichman-Fried M, Maugis B, Grimaldi C, Messerschmidt EM, and Raz E (2015). Dynamic filopodia are required for chemokine-dependent intracellular polarization during guided cell migration in vivo. eLife 4.

Mi H, Muruganujan A, Huang X, Ebert D, Mills C, Guo X, and Thomas PD (2019). Protocol Update for large-scale genome and gene function analysis with the PANTHER classification system (v.14.0). Nat Protoc 14, 703–721. [PubMed: 30804569]

Mineo A, Furriols M, and Casanova J (2018). The trigger (and the restriction) of Torso RTK activation. Open Biol 8, 180180. [PubMed: 30977718]

Minkina A, Lindeman RE, Gearhart MD, Chassot AA, Chaboissier MC, Ghyselinck NB, Bardwell VJ, and Zarkower D (2017). Retinoic acid signaling is dispensable for somatic development and function in the mammalian ovary. Developmental biology 424, 208–220. [PubMed: 28274610]

Motola DL, Cummins CL, Rottiers V, Sharma KK, Li T, Li Y, Suino-Powell K, Xu HE, Auchus RJ, Antebi A, et al. (2006). Identification of ligands for DAF-12 that govern dauer formation and reproduction in C. elegans. Cell 124, 1209–1223. [PubMed: 16529801]

Mukherjee M, Chaudhari SN, Balachandran RS, Vagasi AS, and Kipreos ET (2017). Dafachronic acid inhibits C. elegans germ cell proliferation in a DAF-12-dependent manner. Developmental biology 432, 215–221. [PubMed: 29066181]

Narbonne P, and Roy R (2006). Regulation of germline stem cell proliferation downstream of nutrient sensing. Cell Div 1, 29. [PubMed: 17150096]

Newman AP, White JG, and Sternberg PW (1995). The Caenorhabditis elegans lin-12 gene mediates induction of ventral uterine specialization by the anchor cell. Development 121, 263–271. [PubMed: 7768171]

Newman AP, White JG, and Sternberg PW (1996). Morphogenesis of the C. elegans hermaphrodite uterus. Development 122, 3617–3626. [PubMed: 8951077]

Park KS, Godt D, and Kalderon D (2018). Dissection and Staining of Drosophila Pupal Ovaries. J Vis Exp.

Perkins LA, Holderbaum L, Tao R, Hu Y, Sopko R, McCall K, Yang-Zhou D, Flockhart I, Binari R, Shim HS, et al. (2015). The Transgenic RNAi Project at Harvard Medical School: Resources and Validation. Genetics 201, 843–852. [PubMed: 26320097]

Regan JC, Brandao AS, Leitao AB, Mantas Dias AR, Sucena E, Jacinto A, and Zaidman- Remy A (2013). Steroid hormone signaling is essential to regulate innate immune cells and fight bacterial infection in Drosophila. PLoS Pathog 9, e1003720. [PubMed: 24204269]

Ridley AJ (2011). Life at the leading edge. Cell 145, 1012–1022. [PubMed: 21703446]

Sahut-Barnola I, Dastugue B, and Couderc JL (1996). Terminal filament cell organization in the larval ovary of Drosophila melanogaster: ultrastructural observations and pattern of divisions. Roux Arch Dev Biol 205, 356–363. [PubMed: 28306086]

Sahut-Barnola I, Godt D, Laski FA, and Couderc JL (1995). Drosophila ovary morphogenesis: analysis of terminal filament formation and identification of a gene required for this process. Developmental biology 170, 127–135. [PubMed: 7601303]

Sano H, Kunwar PS, Renault AD, Barbosa V, Clark IB, Ishihara S, Sugimura K, and Lehmann R (2012). The Drosophila actin regulator ENABLED regulates cell shape and orientation during gonad morphogenesis. PloS one 7, e52649. [PubMed: 23300733]

Schulz C, Wood CG, Jones DL, Tazuke SI, and Fuller MT (2002). Signaling from germ cells mediated by the rhomboid homolog stet organizes encapsulation by somatic support cells. Development 129, 4523–4534. [PubMed: 12223409]

Slaidina M, Banisch TU, Gupta S, and Lehmann R (2020). A single-cell atlas of the developing Drosophila ovary identifies follicle stem cell progenitors. Genes & development 34, 239–249. [PubMed: 31919193]

Song X, Wong MD, Kawase E, Xi R, Ding BC, McCarthy JJ, and Xie T (2004). Bmp signals from niche cells directly repress transcription of a differentiation-promoting gene, bag of marbles, in germline stem cells in the Drosophila ovary. Development 131, 1353–1364. [PubMed: 14973291]

Song X, Zhu CH, Doan C, and Xie T (2002). Germline stem cells anchored by adherens junctions in the Drosophila ovary niches. Science 296, 1855–1857. [PubMed: 12052957]

Sower SA, Freamat M, and Kavanaugh SI (2009). The origins of the vertebrate hypothalamic-pituitary-gonadal (HPG) and hypothalamic-pituitary-thyroid (HPT) endocrine systems: new insights from lampreys. Gen Comp Endocrinol 161, 20–29. [PubMed: 19084529]

Sprenger F, and Nusslein-Volhard C (1992). Torso receptor activity is regulated by a diffusible ligand produced at the extracellular terminal regions of the Drosophila egg. Cell 71, 987–1001. [PubMed: 1333890]

Stamatiades GA, and Kaiser UB (2018). Gonadotropin regulation by pulsatile GnRH: Signaling and gene expression. Mol Cell Endocrinol 463, 131–141. [PubMed: 29102564]

Steingrimsson E, Pignoni F, Liaw GJ, and Lengyel JA (1991). Dual role of the Drosophila pattern gene tailless in embryonic termini. Science 254, 418–421. [PubMed: 1925599]

Stoiber M, Celniker S, Cherbas L, Brown B, and Cherbas P (2016). Diverse Hormone Response Networks in 41 Independent Drosophila Cell Lines. G3 (Bethesda) 6, 683–694. [PubMed: 26772746]

Trcek T, Lionnet T, Shroff H, and Lehmann R (2017). mRNA quantification using single molecule FISH in Drosophila embryos. Nat Protoc 12, 1326–1348. [PubMed: 28594816]

Uyehara CM, and McKay DJ (2019). Direct and widespread role for the nuclear receptor EcR in mediating the response to ecdysone in Drosophila. Proceedings of the National Academy of Sciences of the United States of America 116, 9893–9902. [PubMed: 31019084]

Van Doren M, Williamson AL, and Lehmann R (1998). Regulation of zygotic gene expression in Drosophila primordial germ cells. Current biology : CB 8, 243–246. [PubMed: 9501989]

Ventura G, Furriols M, Martin N, Barbosa V, and Casanova J (2010). closca, a new gene required for both Torso RTK activation and vitelline membrane integrity. Germline proteins contribute to Drosophila eggshell composition. Developmental biology 344, 224–232. [PubMed: 20457146]

Wang Z, and Lin H (2004). Nanos maintains germline stem cell self-renewal by preventing differentiation. Science 303, 2016–2019. [PubMed: 14976263]

Warren JT, Yerushalmi Y, Shimell MJ, O'Connor MB, Restifo LL, and Gilbert LI (2006). Discrete pulses of molting hormone, 20-hydroxyecdysone, during late larval development of Drosophila melanogaster: correlations with changes in gene activity. Dev Dyn 235, 315–326. [PubMed: 16273522]

Xiao H, Hrdlicka LA, and Nambu JR (1996). Alternate functions of the single-minded and rhomboid genes in development of the Drosophila ventral neuroectoderm. Mech Dev 58, 65–74. [PubMed: 8887317]

Xie T, and Spradling AC (1998). decapentaplegic is essential for the maintenance and division of germline stem cells in the Drosophila ovary. Cell 94, 251–260. [PubMed: 9695953]

Xie T, and Spradling AC (2000). A niche maintaining germ line stem cells in the Drosophila ovary. Science 290, 328–330. [PubMed: 11030649]

Yamanaka N, Rewitz KF, and O'Connor MB (2013). Ecdysone control of developmental transitions: lessons from Drosophila research. Annu Rev Entomol 58, 497–516. [PubMed: 23072462]

Zhu CH, and Xie T (2003). Clonal expansion of ovarian germline stem cells during niche formation in Drosophila. Development 130, 2579–2588. [PubMed: 12736203]

HIGHLIGHTS

- Steroid pulses coordinate gonadogenesis and primordial germ cell (PGC) differentiation
- An early steroid pulse initiates migration of the swarm cells, a transitory cell type
- A late steroid pulse induces Torso-like, an activator of Torso receptor, in swarm cells
- Torso signaling in PGCs relieves Kr-mediated repression of the differentiation gene *bam*

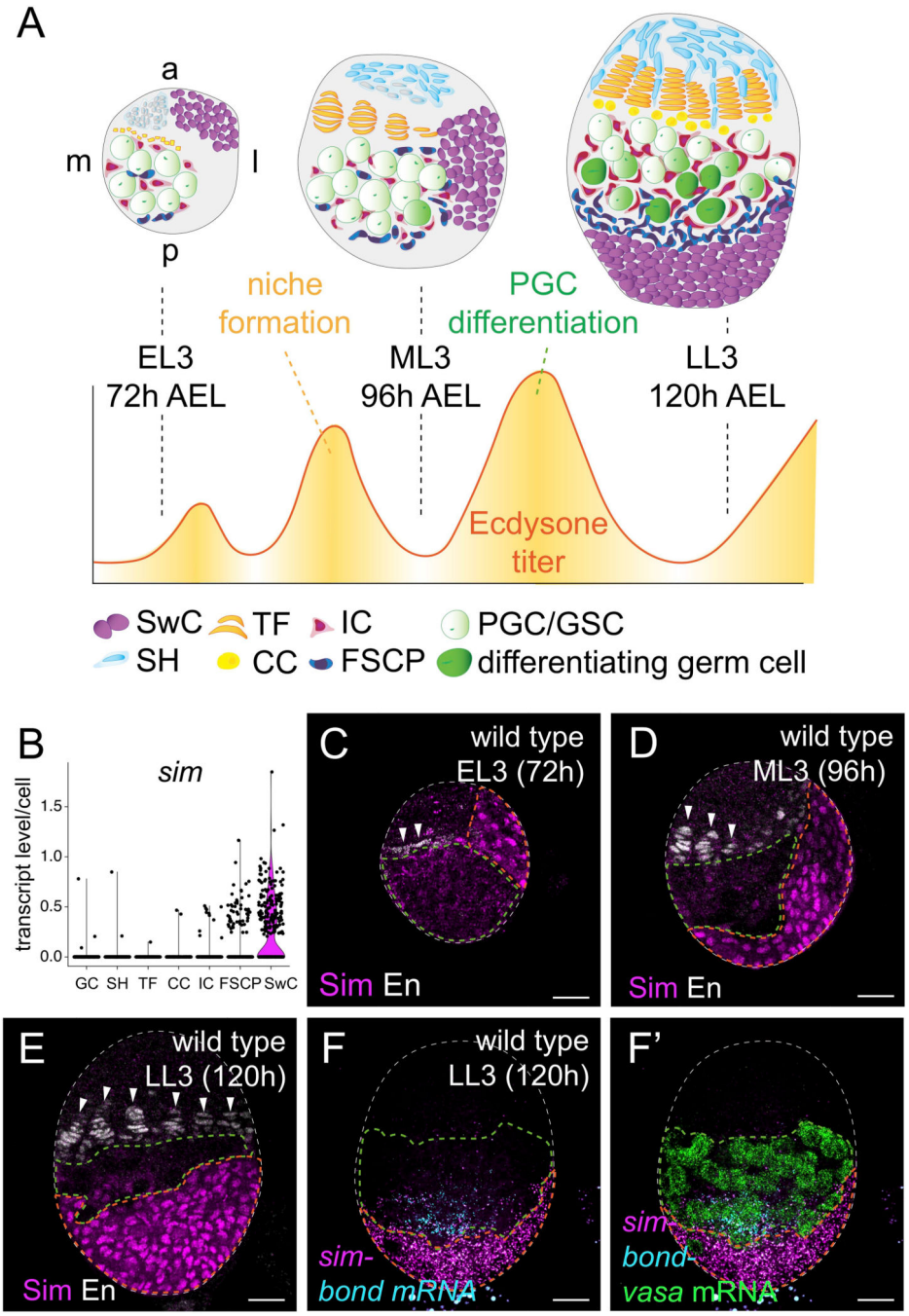

Figure 1. SwC morphogenesis establishes a posterior gonad domain

(A) Schematic of larval ovary development. At EL3 (72h AEL), primordial germ cells (PGCs - light green) proliferate and are in close contact with intermingled cells (ICs - red) and follicle stem cell progenitors (FSCPs - dark blue). Terminal filament progenitors (TFs - orange) and sheath cells (SH - light blue) are specified at the anterior; swarm cells (SwCs - purple) are located anterolateral. An early ecdysone peak (~90h AEL) induces niche formation, SwCs are located dorsolateral. A late ecdysone peak (~100h AEL) initiates PGC differentiation (dark green); whereas PGCs close to the forming niches (TFs and cap cells

(CC) - yellow) are maintained as germline stem cells (GSCs); SwCs form a posterior domain. (B) Violin plot from scRNA-seq. data for *sim;* gene expression levels (y axis) for each ovarian cell cluster (x axis) are given, each dot represents a cell. (C-E) Anti-Sim antibody detects SwCs (orange outline) during development. TF morphogenesis (arrowheads) marked by anti-Engrailed (En) antibody (white) marks developmental stages; PGC compartment is green outlined. (F) Spatial relationship of PGCs *(vasa),* FSCPs *(bond)* and SwCs (sim), detected by HCR *in-situ* hybridization at LL3. Scale bars indicate 10 μm. See also Figure S1.

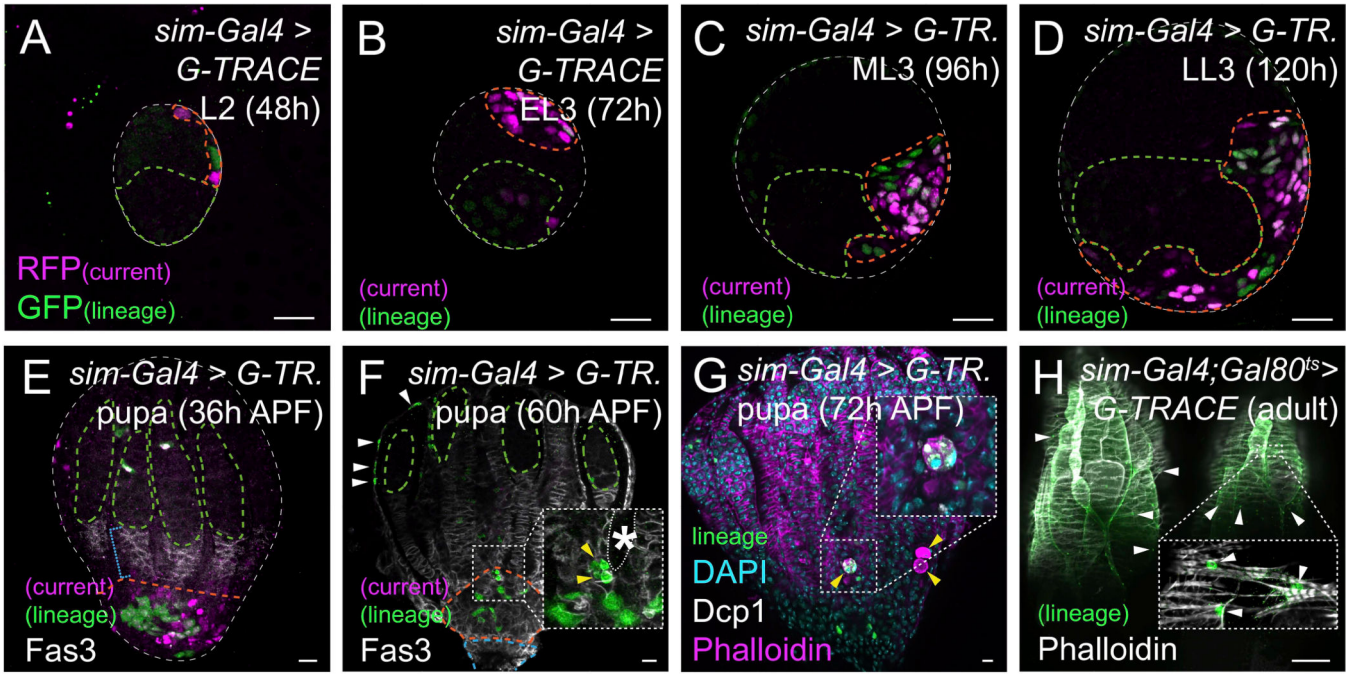

Figure 2. Lineage tracing reveals transitory nature of SwCs

(A-H) sim-Gal4 driven expression of G-TRACE follows SwC fate: current (RFP in magenta) and lineage expression (GFP in green); SwC locations and PGC positions are marked by orange and green outline, respectively. (A-G) Current expression reveals sim-Gal4 activity in SwCs from L2 on, recapitulating SwC morphogenesis. In pupae, by 60h APF current expression can no longer be detected. (E-F) At 36h-60h APF, SwC descendants are found at the posterior separated from PGCs (green outline) by follicle cells labeled with anti-Fasciclin3 antibodies (Fas3) (blue bracket). (F) By 60h APF SwC lineage contributes to the calyx (blue outlined); few lineage-labeled cells can be found in the developing peritoneal sheath (white arrowheads). (F-G) SwCs at the base of developing ovarioles (yellow arrowheads in insets; asterisk and white outline mark extra-ovariolar cavity in F) undergo apoptosis marked by anti-Dcp-1 antibodies (G). (H) Larval SwCs descendants were detected in the peritoneal sheath (Phalloidin, arrowheads) of adults. Scale bar indicates 10 μm, except 100 μm in H. See also Figure S1.

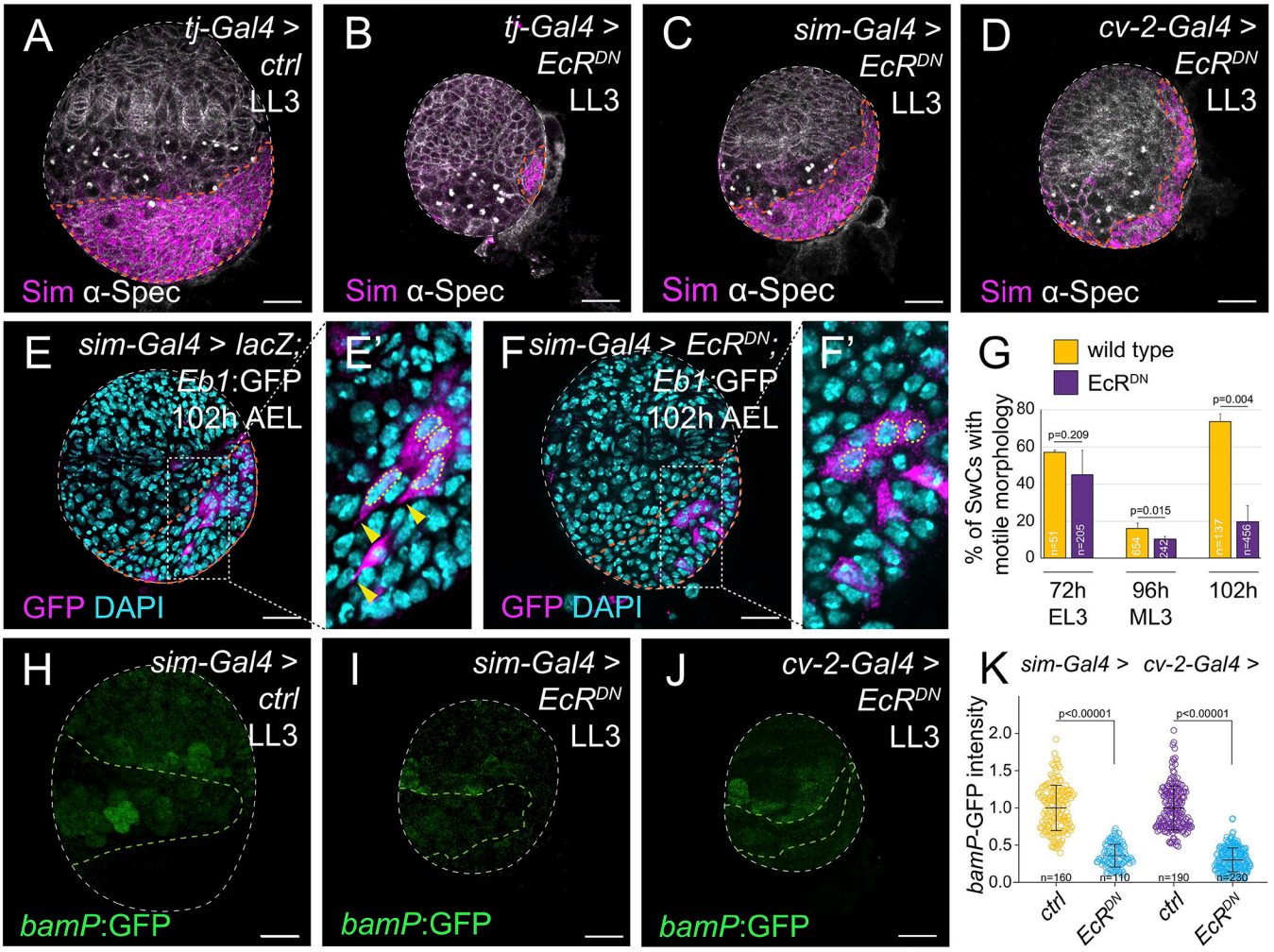

Figure 3. Ecdysone pulses promote SwC morphogenesis and PGC differentiation

(A-D) Effect of EcR^{DN} expression on SwC morphogenesis. SwCs are labeled with anti-Sim antibodies (orange outline); all cell outlines and the fusome in PGCs are marked by anti-α-Spectrin. (A) SwCs occupy the posterior in control ovaries at LL3; (B) pan-somatic *(tj-Gal4)* or (C and D) SwCs specific (sim-Gal4, *cv-2-Gal4)* expression of EcR^{DN} impacts SwC morphogenesis. (E-F) Eb1:GFP marks SwC protrusions and DAPI marks nuclear morphology. (E-E') Wildtype SwCs initiate posterior migration shortly after ML3, indicated by directional protrusions and elongated nuclear morphology (arrowheads and outline). (F) SwCs expressing EcR^{DN} lack motile behavior. (G) Graphical representation of SwC motility index in control and EcR^{DN} expressing SwCs. (H-J) PGC differentiation is monitored by *bamP:GFP,* PGC domain is outlined in green. (H) Wildtype PGCs initiate differentiation at LL3; (I-J) *bamP:*GFP reporter expression is absent in EcR^{DN} expressing SwCs (note, *bamP:*GFP reporter shows ectopic expression in TFs). (K) Graph depicting relative *bamP:*GFP expression levels as exemplified in H-J. Each data point represents a single PGC. Error bars represent SD. Scale bars indicate 10 μm. See also Figure S2.

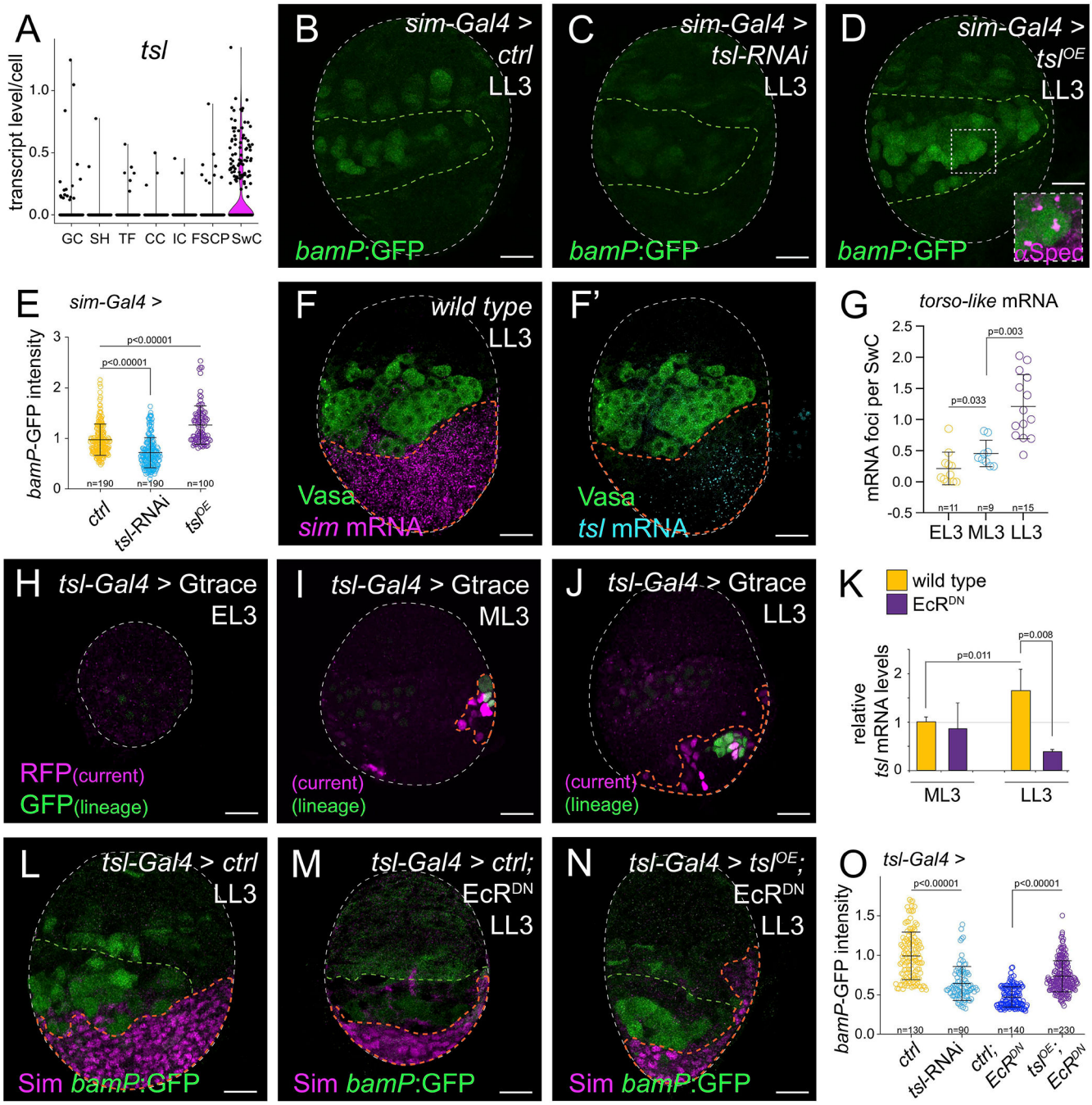

Figure 4. SwCs express *tsl* to initiate PGC differentiation in response to a late larval ecdysone pulse

(A) Violin plot from scRNA-seq. data for *tsl;* gene expression levels (y axis) for each ovarian cell cluster (x axis) are given, each dot represents a cell. (B-D) PGC differentiation status is indicated by *bamP:*GFP expression; PGC domain is outlined in green. (B) PGCs in control ovaries express *bamP:*GFP. In tsl-RNAi knock-down (C) *bamP:*GFP expression was decreased, in *tsl*^{E} (D) *bamP:*GFP expression was increased. Precocious PGC differentiation is highlighted by presence of branched fusomes (anti-a-Spectrin, inset). (E) Graph quantifying *bamP:*GFP expression levels as exemplified in B-D. Each data point represents a

single PGC. (F, F') HCR *in-situ* hybridization for *tsl* and *sim* mRNAs at LL3, germ cells are labeled with anti-Vasa antibodies. (G) Graph showing average number of *tsl* mRNA foci per SwC at EL3 to LL3; each data-point represents a single ovary. (H-J) tsl-Gal4 driven expression of G-TRACE. No expression was detected at EL3, few SwCs were labeled at ML3 and many were labeled at LL3. (K) qPCR measurements showing increased *tsl* mRNA levels from ML3 to LL3 in wildtype, but not when EcR^{DN} was expressed in soma. (L-N) SwCs are marked *via* anti-Sim antibodies (orange outline), PGC differentiation status is indicated by bamP:GFP (PGC domain outlined in green). (L-M) tsl-Gal4 driven EcR^{DN}: SwC migration was unaffected but PGC differentiation was blocked. (N) Reintroduction of *tsl* rescued the EcR^{DN} phenotype. (O) Graph depicting relative *bamP:*GFP expression levels as exemplified in L-N. Each data point represents a single PGC. Error bars represent SD. Scale bar indicates 10 μm. See also Figure S2.

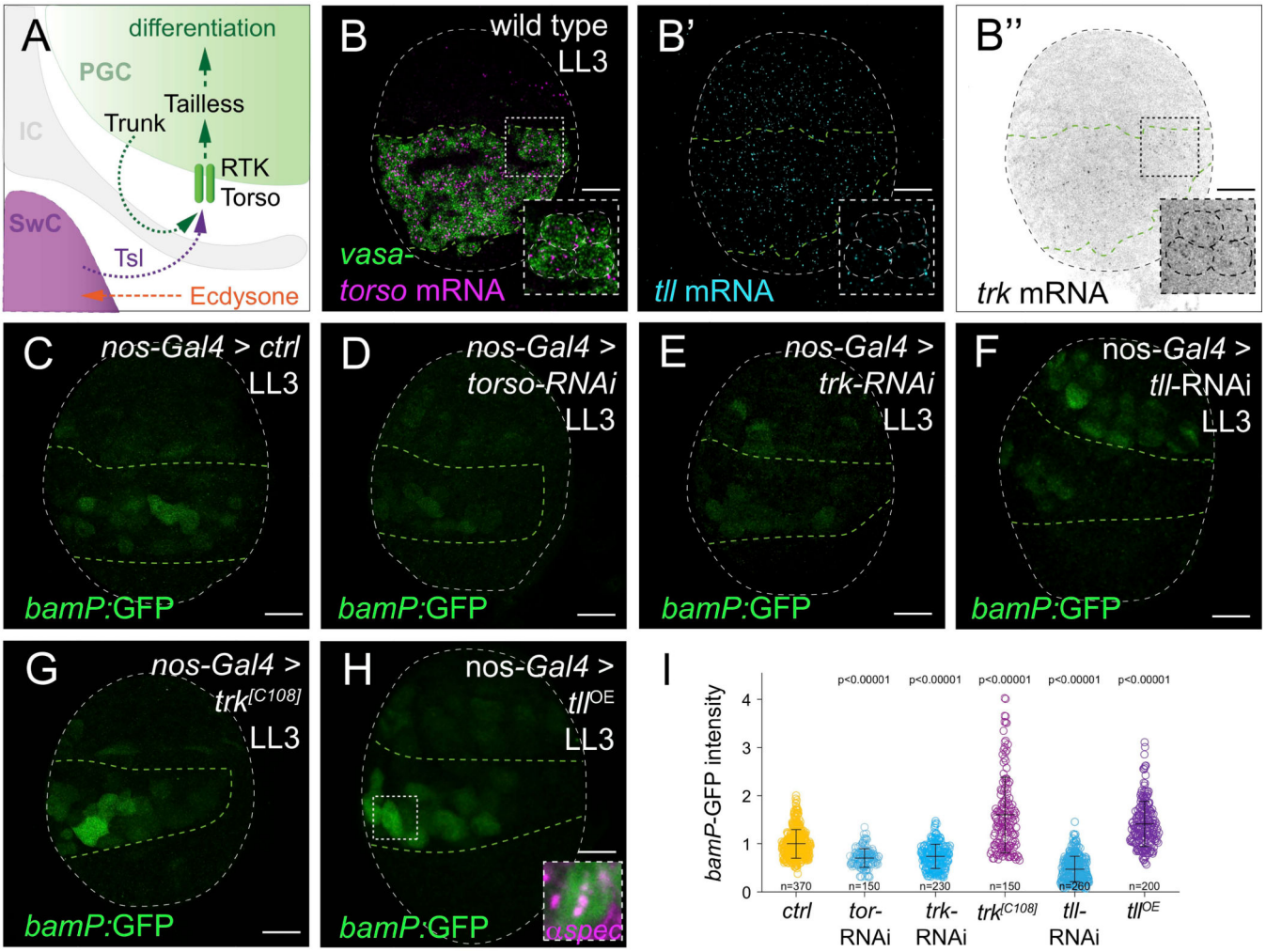

Figure 5. Temporal control of Tsl expression in SwCs promotes PGCs differentiation via RTK Torso signaling

(A) Schematic summary of SwC-to-PGC signaling via Tsl-Torso pathway. (B) HCR *in-situ* hybridizations for *torso, trk, tll* and *vasa* mRNAs. (C-H) PGC differentiation status is indicated by *bamP:*GFP; PGC domain is outlined in green. RNAi-mediated knock-down of *torso* (D), *trk* (E), or *tll* (F), resulted in decreased bamP:GFP expression when compared to control. Expression of an activated version of *trk* (*trk*$^{[C108]}$) (G), and overexpression of *tll* (H), resulted in precocious PGC differentiation, highlighted by presence of branched fusomes (anti-a-Spectrin, inset). (I) Graph depicting relative bamP:GFP expression levels as exemplified in C-H. Each data point represents a single PGC; P values in relation to control. Error bars represent SD. Scale bar indicates 10 μm. See also Figure S3.

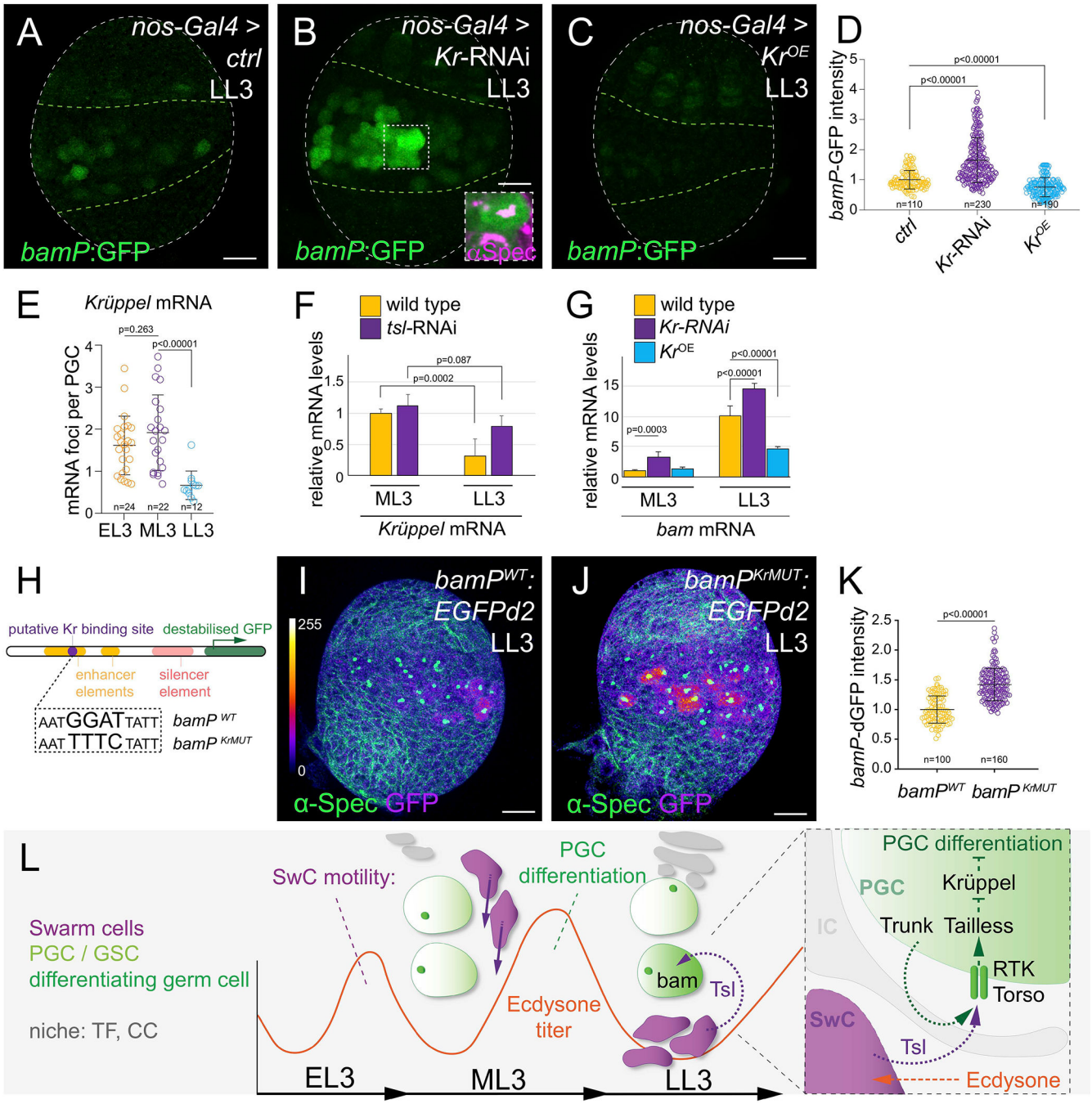

Figure 6. Torso pathway promotes PGCs differentiation by alleviating Krüppel-mediated repression of *bam* promoter activity.

(A-C) bamP:GFP expression indicates PGC differentiation status, PGC domain is outlined in green. (B) PGC specific *Kr*-RNAi knockdown results in precocious differentiation highlighted by presence of branched fusomes (anti-a-Spectrin, inset), (C) *Kr* blocks differentiation. (D) Graph depicting relative *bamP:*GFP expression levels as shown in A-C. Each data point represents a single PGC. (E) Measurements of *Kr* mRNA foci detected by HCR in PGCs at EL3 to LL3; each data-point represents a single ovary. (F) qPCR measurements show decrease of *Kr* mRNA levels from ML3 to LL3 in wild type gonads but

not when tsl-RNAi was expressed in soma. (G) qPCR measurement of *bam* mRNA levels, showing significant increase from ML3 to LL3 in wildtype. Kr-RNAi in PGCs results in elevated *bam* levels at ML3 while Kr^{OE} decreased *bam* levels at LL3. (H) Schematic representation of *bam* transcriptional reporters. In $bamP^{wt}$:EGFPd2, the *bam* promoter sequence was fused to a destabilized EGFP; known enhancer elements (orange) and the Mad/Med targeted silencer element (red) are indicated. In $bamP^{krmut}$:EGFPd2A a putative Kr binding site (purple) was mutated. (I-J) Reporter expression is increased when the Kr binding site is mutated. (K) Graph depicting relative expression levels of the *bam* reporters as exemplified in I-J. Each data point represents a single PGC; Error bars represent SD. Scale bar indicates 10 μm. (L) Model for ecdysone control of SwC morphogenesis and PGC signaling. See also Figure S4.

KEY RESOURCE TABLE

REAGENT or RESOURCE	SOURCE	IDENTIFIER
Antibodies		
chicken anti GFP (1:500)	Aves Labs Cat# GFP-1020	RRID:AB_10000240
rat anti RFP (1:500)	ChromoTek Cat# 5f8–100	RRID:AB_2336064
guinea pig anti Tj (1:7000)	Prof. Dorothea Godt	
mouse anti Fas3 (1:4)	DSHB Cat# 7G10 anti-Fasciclin III	RRID:AB_528238
mouse anti a-Spectrin (1:100)	DSHB Cat# 3A9 (323 or M10–2)	RRID:AB_528473
rabbit anti Vasa (1:5000)	Lehmann Lab	
rabbit anti cleaved Dcp-1 (1:100)	Cell Signaling Technology Cat# 9578	RRID:AB_2721060
rabbit anti pMad (1:500)	Prof. Edward Laufer	
guinea pig anti Sim (1:50)	Prof. Steven Crews	
mouse anti Engrailed (1:20)	DSHB Cat# 4D9 anti-engrailed/invected	RRID:AB_528224
Alexa Fluor 488 Phalloidin	Thermo Fischer Sc.	# A12379
Experimental models: organisms/strains		
w^{1118}	Lehmann lab stock	
G-TRACE: w[*]; P{w[+mC]=UAS-RedStinger}4, P{w[+mC]=UAS-FLP.D}JD1, P{w[+mC]=Ubi-p63E(FRT.STOP)Stinger}9F6/CyO	(Evans et al., 2009)	BDSC # 28280
G-TRACE: w[*]; P{w[+mC]=UAS-RedStinger}6, P{w[+mC]=UAS-FLP.Exel}3, P{w[+mC]=Ubi-p63E(FRT.STOP)Stinger}15F2	(Evans et al., 2009)	BDSC # 28281
w[*]; P{w[+mC]=UAS-EB1-GFP}3		BDSC # 35512
sim-Gal4: w[*]; P{w[+mC]=GAL4-sim.3.7}2/CyO; P{w[+mC]=GAL4-sim.3.7}3	(Xiao et al., 1996)	BDSC # 9150
traffic jam-Gal4: [P(GawB)NP1624]		DGRC # 104055
P{GAL4::VP16-nos.UTR}	(Van Doren et al., 1998)	
cv-2-Gal4: Mi{Trojan-GAL4.1}cv-2[MI10363-TG4.1]	(Lee et al., 2018)	BDSC #67491
tsl(B)-Gal4	(Furriols et al., 2007)	
bamP:GFP: P{-898/+133-bam:GFP}	(Chen and McKearin, 2003b)	
lacZ: P{UAS-lacZ.B}Bg4–2–4b	(Brand and Perrimon, 1993)	BDSC #1777
EcR^{DN}: P{UAS-EcR.A.W650A}TP5		BDSC #9451
$Gal80^{ts}$: P{tubP-GAL80[ts]}ncd[GAL80ts-7]	(McGuire et al., 2003)	BDSC #7018
tsl-RNAi: P{TRiP.HMC04408}attP40	(Perkins et al., 2015)	BDSC #56967
tsl-RNAi : *UAS-tsl-RNAi 42*	(Furriols et al., 2007)	
tsl^{OE}*: UAS-Tsl (WT 2.1)*	(Furriols et al., 2007)	
torso-RNAi: w^{1118}; P{GD14396}v36280		VDRC #v36280
trunk-RNAi: y^1 sc* v^1 sev^{21}; P{TRiP.HMC04348}attP40	(Perkins et al., 2015)	BDSC #56040
pUAST-trk [C108]	(Casali and Casanova, 2001)	
tll-RNAi: y^1 v^1; P{TRiP.JF02545}attP2	(Perkins et al., 2015)	BDSC #27242
tll^{OE}: M{UAS-tll.ORF.3xHA.GW}ZH-86Fb	(Bischof et al., 2013)	FlyORF # F000061
Kr-RNAi: P{TRiP.JF02745}	(Perkins et al., 2015)	BDSC #27666

REAGENT or RESOURCE	SOURCE	IDENTIFIER
Kr^{OE}: M{UAS-Kr.ORF.3xHA.GW}Zh-86Fb	(Bischof et al., 2013)	FlyORF # F000584
w;;*bamP WT:destabilized EGFP:bam3'UTR*	this study	
w;;*bamP KrMut:destabilized EGFP:bam3'UTR*	this study	
Oligonucleotides		
rps17 fw	CAAGATTGCCGGCTATGTCA	
rps17 rv	CCTGCAACTTGATGGAGATACCA	
tsl fw	CAATGACAACTCGGAGCC	
tsl rv	ATCGCCTTGGATGAAAGATG	
trk fw	GCTCACTTGGTTGGCAGT	
trk rv	GCTCTTCTCCTCGGGCT	
torso fw	GTTTGGTCCTTTGGTTGTCT	
torso rv	TAAGGGCGGAAAATGTTG	
kr fw	CGAGGCATCCAGGAATAGAT	
kr rv	CACTGGGTACGTGAGGGATT	
bam fw	GCACATCGGGCGTTTTATCC	
bam rv	CGAACAGATAGTCCGAGGGC	